

Investigating the optimal environment for CO₂ Plume Geothermal

Sjoerd Akkermans

Investigating the optimal environment for CO₂ Plume Geothermal

by

Sjoerd Akkermans

Thesis Committee:

Chair:

Denis Voskov

Reservoir Engineering

Committee Member:

Alexandros Daniilidis

Reservoir Engineering

Committee Member:

Guillaume Rongier

Applied Geology

Faculty:

Faculty of Civil Engineering and Geosciences

Abstract

Multiple studies have shown the potential for CO_2 plume geothermal (CPG) to be a sustainable, reliable energy source that can be utilized in numerous regions worldwide. Compared to conventional brine-based systems, a significant benefit is that CO_2 allows for direct electricity generation at lower temperatures than brine. It could serve as both a continuous source of energy generation and a dispatchable source when energy demand is high. In addition, it could serve as a pre-carbon capture and sequestration (CCS) phase. Where it could verify the integrity of the reservoir and acquire information to characterize the reservoir and understand its behaviour under CO_2 injection. Before a proof-of-concept site can be chosen, candidate fields should be evaluated to find the optimal environment for CPG. In this work, we investigate which systems, aquifer or gasfield, injection-production scheme and what kind of environment provide the best performance for CPG. We use the Open Delft Advanced Research Terra Simulator (Open-DARTS) to simulate this on a reservoir scale. Open-DARTS uses the Operator-Based Linearization (OBL) approach to model all non-linear physics involved. To get an estimate of the electricity and heat generated by the system, we extend the open-DARTs framework to include a simple wellbore model and surface infrastructure. In our results, we look at the performance of two types of reservoirs: aquifers and gas fields. Where we consider the amount of electricity generated energy and other performance metrics. We find major differences between CPG performance in aquifers and gas fields. The results show that maintaining steady electrical energy generation through a CO_2 production in an aquifer appears to be much easier than it is for gas fields. With Aquifers consistently having a higher water cut. Furthermore, the inclusion of a plume establishment (PE) phase does boost performance once the CPG stage starts for both the aquifer and gas field types.

Acknowledgements

When I started this master's program two years ago, with no background in earth sciences, it was quite a leap in the dark. Two years later, I can confidently say I made the right decision. I found an incredibly passionate and positive faculty, which was more than willing to help catch up on geology every step of the way. Following this master's programme has been a delightful experience.

First of all, I would like to thank my supervisor, Denis Voskov. Throughout the project, Denis has been a pillar of support. Our weekly meetings were consistently incredibly insightful, and he always seemed to have a solution to whatever problem I encountered. Denis's confidence and support have made working on this thesis a very gratifying endeavor. His inclusion of me in his weekly DARTS group meetings has also been great. Looking back at the first meeting, where I did not understand a single thing that was discussed. Compared to now, where I can understand and engage in most topics. Which is really a testament to how much I have learned during my time at Denis' group.

During many of these weekly meetings, Alexandros Daniilidis and Boyukagha "Agha" Baghirov were present to support me with their insights. Their feedback and ideas often helped me notice my blind spots and find the path forward. I am very thankful for their help making this thesis possible.

This work would not have been possible without Michiel Wapperom, besides relying for a significant part on his work through DARTS-Flash. He helped me in numerous ways and was always available to answer my questions, help me out, or lend me his campus card to get free coffee.

Guillaume Rongier, next to being one of my committee members, has been great teacher during this master's. I particularly enjoyed his course in the modelling of geological heterogeneities. That I could transfer my knowledge of electrical signals to modelling permeabilities of fluvial systems remains one the biggest eye openers during this master's.

I want to thank my incredible girlfriend, Rosa, who has supported me tremendously throughout this project. Throughout the project she has always available to help me and she has supported me in countless ways, from proofreading my work to making me many delicious dinners in the last few stressful weeks of this project. I could not have done it without her.

Lastly, I want to thank all the people I have met and come to love here in Delft. Your incredible confidence in me and the countless lunches and coffee break visits (even on Sundays) are deeply appreciated.

Contents

Preface	i
Summary	ii
1 Introduction	1
1.1 Current research	1
1.2 Problem Statement	2
1.3 Thesis structure	2
2 Background	3
2.1 Why CPG	3
2.2 Thermosiphon effect	3
2.2.1 Flow-regime	5
2.3 Literature review on Reservoirs	7
2.3.1 Saline Aquifers	7
2.3.2 (Depleted) Gasfields	8
3 Methodology	9
3.1 Reservoir model	9
3.1.1 Gridding	9
3.1.2 Component selection	9
3.2 Multiphase-flow through porous media	9
3.2.1 Heat conduction and convection through porous media	10
3.2.2 Thermodynamics	10
3.2.3 Properties	12
3.3 Thermodynamic Cycle	14
3.3.1 Modelling Isentropic processes	14
3.3.2 Cycle components	14
3.3.3 Wellhead to bottom hole (State 1 to 2)	15
3.3.4 Reservoir (State 2 to 3)	16
3.3.5 Bottom hole to wellhead (State 3 to 4)	16
3.3.6 Turbine (State 4 to 5)	16
3.3.7 Condenser	16
3.4 Cycle evaluation	17
3.5 Operator Based Linearization	18
3.5.1 Operator Expansion	18
3.6 Phase transitions	20
3.7 Parameters	21
3.8 Performance metrics	21
3.9 Gains from our method	23
4 Verification	26
4.1 Aquifer verification	26
4.2 Gasfield validation	28
4.3 Regarding other simulators	29
4.3.1 THOUGH2	29
4.3.2 CMG-GEM	29
4.3.3 Open-DARTS comparison	30
5 Simulation strategy	31
5.1 PE phase	31

5.2	Wells	31
5.3	Simulation parameters	31
5.4	Experimentation plan	32
5.4.1	Reservoir type comparison	33
5.4.2	Injection-production scheme	33
5.4.3	Study of the environment	33
6	Results	35
6.1	Base case	35
6.1.1	Aquifer	35
6.1.2	Gasfield	38
6.2	Great Aquifer	40
6.2.1	Aquifer	40
6.2.2	Gas field	40
6.3	Plume establishment	41
6.3.1	Aquifer	41
6.3.2	Gas field	43
6.4	Seasonal electricity	43
6.5	Stratified geology	45
7	Discussion	47
8	Conclusion and recommendations	49
	References	51

1

Introduction

With the effects of increased levels of greenhouse gasses in the atmosphere becoming more apparent in the last decades, the already strong societal call to reduce emissions is only getting stronger. So far, human-induced global warming has caused global temperatures to rise by 1.1° C. The Intergovernmental Panel on Climate Change (IPCC) presented several pathways to limit this warming to 1.5° C. In all these pathways, the IPCC demands strong upscaling of renewables and rapid deployment of carbon capture and sequestration (CCS) technologies is required [56]. CCS is the practice of capturing the carbon emissions from industrial processes and storing them underground. Thereby mitigating the environmental impact of these processes.

One of these possible renewable energy sources is geothermal energy. This technology harnesses the heat from the earth's subsurface to generate electricity or provide heat. A form of geothermal, CO_2 Plume Geothermal (CPG), synergizes this energy source with CCS. Not only does this technology encourage CCS, but it also benefits from faster and more efficient heat extraction than conventional, water-based geothermal systems. By injecting the polluting CO_2 emissions from big emitters and then producing a part of this after being heated within the reservoir, a turbine can be fueled to produce electricity.

Heat extraction from the subsurface using supercritical CO_2 was initially proposed by Donald Brown in 2000 [10]. Jimmy B Randolph and Martin O Saar first proposed the combination of geothermal and CCS in 2011, and coined the term CPG [53]. Extensive research has been done since, including one field test. In 2023, a consortium was founded to establish a field demonstration of this technology. While this consortium is still in its feasibility phase, the next phase will be field selection.

Various reservoirs have been proposed and studied as possible targets for CPG. Aquifers, as a popular target for CCS projects, have often been suggested as good targets. Additionally, synergy with pre-CCS use of reservoirs, such as hydrocarbon extraction in the context of EOR or EGR, has also been studied with promising theoretical results. However, quantitative and qualitative comparisons of environments have still not been done. In this study, we utilize and expand upon the open Delft Advanced Research Terra Simulator (open-DARTS) framework to study CPG systems and compare them based on determined parameters.

1.1. Current research

One of the earliest studies quantifying the benefits of CPG is the study done by Adams et al. using the TOUGH2 simulator [3]. It substantiated the theoretical benefits of CPG over conventional geothermal with numerical results. These benefits include that CO_2 suffers from considerably fewer pressure losses than brine-based systems and greater flow rates driven by the thermosiphon effect, and through this, a significantly reduced need for pumping power.

An important field experiment was done in 2015, which aimed to establish a thermosiphon successfully [30]. This experiment did not yield the expected results, and later analysis postulated that the accu-

mulation of high-density water in the production well caused the density difference between the two wells to diminish. Following these initial studies Ezekiel, in his dissertation and accompanying papers, explores the feasibility of CPG in gas reservoirs. Including a possible synergy with EGR [24]. Saline aquifers as a popular target or CCS have also been studied by Norouzi et al. [45]. This study focuses on the performance of fluvial aquifers, a type of reservoir that is commonly found around the world, including in the southern Dutch North Sea.

1.2. Problem Statement

Research done previously shows us a wide range of possible candidate reservoirs for CPG, such as aquifers [45], gas-fields [24], or oil-fields [33]. Reservoir modelling and techno-economic analyses have been done to show theoretical profitability, and several sensitivity analyses have been done on how reservoir parameters impact this [2] [24]. What has not been done is a direct comparison of the performance of all these systems under a unified framework; this leads us to our research question:

The optimal environment for CPG performance: which systems, stages of development and physical parameters provide the best performance?

1. How do the different types of reservoirs, aquifers, and gas fields, compare?
2. How does the injection-production scheme impact performance?
3. How does the environment of the reservoir influence performance?

To answer these questions, we build a model using the open-DARTS framework. In a previous master thesis using open-DARTS, the decision was made to neglect all parts of the cycle except for the reservoir [7]. That thesis focused on how heterogeneities impacted flow. This thesis, however, aims to compare the performance of reservoirs, and therefore the evaluation of the whole cycle is deemed necessary to approximate the electricity produced. Furthermore, following the findings of Fleming et al. regarding water exsolution, the importance of a multiphase multicomponent approach over the entire cycle is required. Our approach will be:

- Build an open-DARTS reservoir model
- Build a simplified approximation of the cycle
- Validate model with literature
- Quantify key parameters to judge and compare reservoir performance
- Run simulations for different types of reservoirs
- compare performances and identify differences.

1.3. Thesis structure

The structure of this master thesis is as follows:

- Chapter 1: Introduction and problem statement
- Chapter 2: Background information
- Chapter 3: Methodology and elaboration on the model
- Chapter 4: Validation study
- Chapter 5: Simulation strategy
- Chapter 6: Results
- Chapter 7: Discussion
- Chapter 8: Conclusion and recommendations

2

Background

2.1. Why CPG

CPG has several benefits over conventional brine-based geothermal systems. For example CO_2 as a working fluid has higher mobility and lower solubility of amorphous silica, but maybe less trivial, a higher density sensitivity to temperature. The density of the CO_2 changes significantly during its path from the reservoir to the surface plant. This causes a buoyancy-driven convective current, which we refer to as a thermosiphon effect. This effect greatly reduces the pumping load necessary and thus increases the efficiency of the energy extraction [3].

The influential study, “On the importance of the thermosiphon effect in CPG (CO₂ plume geothermal) power systems”, written by Adams et al. about the most important benefits of CPG can be summarized as follows [3]:

- **Less pressures losses for CO_2 than for brine.** Flow in the reservoir causes a pressure drop in the fluid. This pressure drop is proportional to the average specific inverse mobility (M). This value is 3-12 times lower for CO_2 than for brine. M is dependent on the dynamic viscosity of the fluid, which is temperature and thus depth related for brine but is roughly constant for CO_2 —making it a more efficient working fluid.
- **The thermosiphon-induced by the CO_2 creates a greater mass flowrate than brine.** The CO_2 is near its critical point during circulation, causing it to be very sensitive to changes in temperature and pressure. This in turn causes a big difference in density in the injection and production well creating the thermosiphon effect. This generates a significant thermosiphon force from depths as shallow as 0.5 km. At higher depths with higher temperatures, the flow rate of brine eventually does comes closer to that of CO_2 .
- **The thermosiphon effect drives the convection, greatly reducing the need for pumping power.** Through the thermosiphon effect the CO_2 directly uses the energy extracted to drive its circulation. This diminishes the need for pumping power, or in some cases eliminates it entirely.

In addition to these reservoir-sided benefits, another major advantage is at the surface.

- **Significantly more electricity production at shallow reservoirs.** Conventional geothermal requires relatively high temperatures or ORC units to produce electricity from geothermal resources. CO_2 , on the other hand, can directly be used in turbines for electricity generation. This creates a much bigger share of electricity at equivalent (shallow) reservoir conditions [32].

2.2. Thermosiphon effect

One major advantage of CPG over conventional geothermal systems is the thermosiphon potential over a wider range of conditions than brine-based systems. CO_2 's density is very sensitive to temperature changes, especially around reservoir conditions. In figure 2.1, the density as a function of temperature and pressure is plotted. The gas-liquid boundary can clearly be distinguished up to the critical point,

after which it is considered to be in the supercritical phase. For the thermosiphon forcings, the temperature dependence of the density is the factor influencing its strength. In figure 2.2, the density of CO_2 is given at several reservoir pressures. For these figures and the rest of this report, we will use the DARTS-flash package [47] for thermodynamic properties.

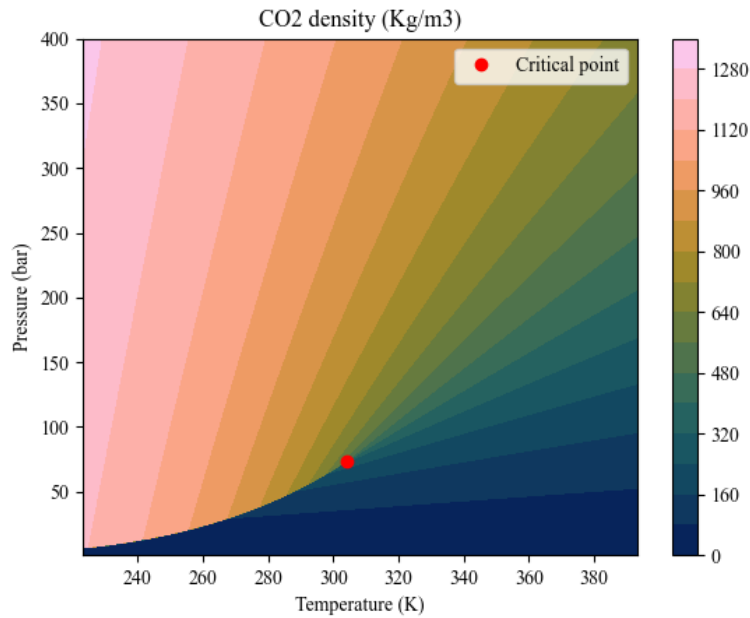


Figure 2.1: The density of pure CO_2 plotted as a function of pressure and temperature.

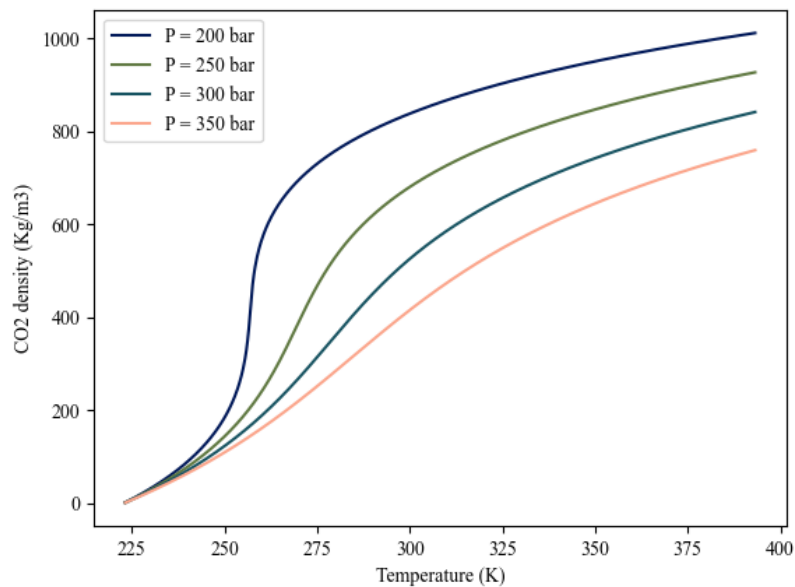


Figure 2.2: The density of pure CO_2 plotted as a function of temperature at several isobars.

The aforementioned density difference comes to fruition in the boreholes. The hydrostatic pressure drop over the injection and production well will be different, as the temperature and, thus, densities will

differ significantly. If friction losses are to be neglected, the hydrostatic pressure gradient is given as in equation 2.1. Ideally, you can treat the CO_2 flow through the boreholes as an isentropic expansion [55] and thus for every dz its temperature and pressure will change (and with that ρ_{CO_2}).

$$\int_{P_{z_1}}^{P_{z_2}} \frac{1}{g\rho(P, T)} dP = z_2 - z_1 \quad (2.1)$$

For a reservoir at 2.5 km depth with the corresponding state of 250 bar and 100 °C the hydrostatic pressure gradient differs within each borehole. As can be seen in figure 2.3, there is a pressure differential in the preferred direction both at the surface and at the reservoir depth. This will drive convection both in the reservoir and on the surface. This is what is referred to as the thermosiphon effect.

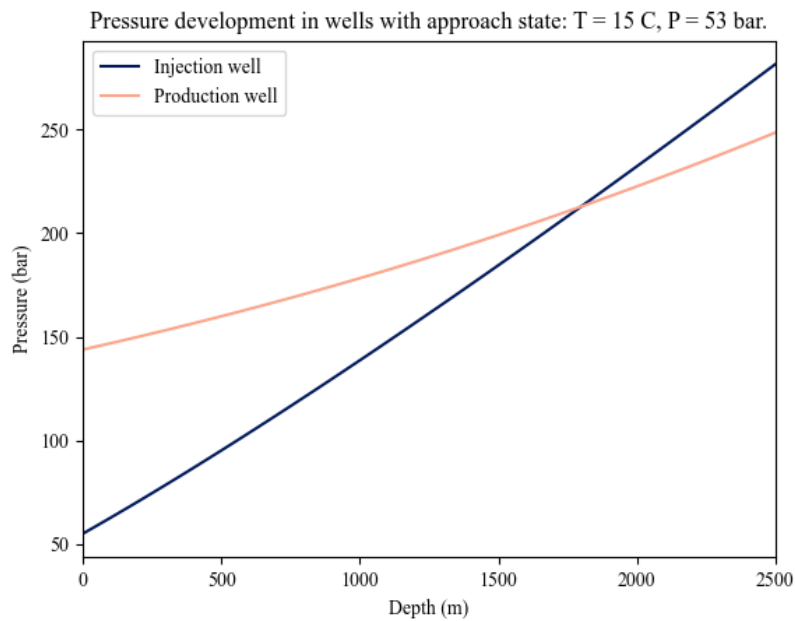


Figure 2.3: Pressure in both wells under isentropic conditions.

2.2.1. Flow-regime

To test the concept of the thermosiphon effect an experiment was done in 2015 at the South Eastern Regional Partnership for Carbon Sequestration (SECARB) Cranfield site in the USA [30]. The SECARB site has been used previously for experiments with CO_2 storage. The reservoir is located at 3.2 km depth and had a temperature of roughly 127° C. Based on previously done simulations, they expected to be able to generate a self-sustaining thermosiphon flow; however, during their experiment, their flowrates consistently kept decreasing, as can be seen in figure 2.4. So, they failed to demonstrate the self-sustaining thermosiphon effect in the context of CPG.

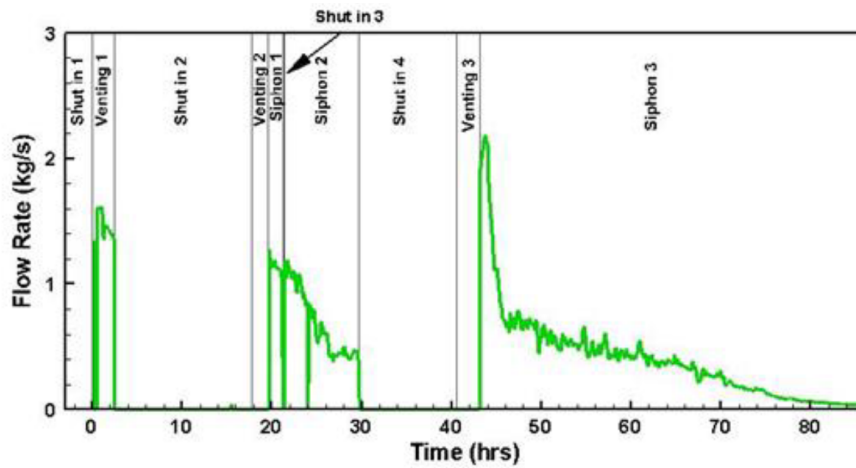


Figure 2.4: Results of SECARB test figure from [30].

Multiple causes why this experiment has failed have been proposed. Generally, they agree that a too-low flow speed and accumulation of high-density water within the production borehole appear to be the main culprits [1][23]. It is postulated that a slug or churn flow regime within the borehole, which appears at too low gas velocities and too high volume fractions of water, could be the reason for failure. Because of this and as done in recent studies [23] [60], we will take annular flow as a requirement for CPG production. This is relevant as this flow regime reduces the pressure drop over the production well and favours gas production over water production. To determine the flow regime within the well-bore, we use the model outlined by Taitel, Barnea, and Dukler. This theoretical model corresponds to experimental data and is used in multiple recent CPG studies [23]. For our purposes, we use the flow regime boundary as a function of the gas flow speed, which is given by equation 2.2.

$$\frac{Q_V}{\pi R^2} V_{CO_2} \sqrt{\rho_V} = 3.1 \sigma (\rho_{Aq} - \rho_V)^{1/4} \quad (2.2)$$

Where Q_V is the amount of vapour phase produced, R the radius of the borehole, V_V the volume fraction of the vapour phase, ρ_V the density of the vapour phase and ρ_{Aq} the density of the aqueous phase and σ the interfacial tension.

While the SECARB experiment failed, claims have been made by private companies that a thermosiphon has been successfully established in a depleted gasfield [8]. However, given the minimal data published about this experiment, it is hard to confirm its validity and details of the operation. Therefore the SECARB experiment still stands as the most informative experiment on the thermosiphon effect in the context of CO_2 Plume Geothermal.

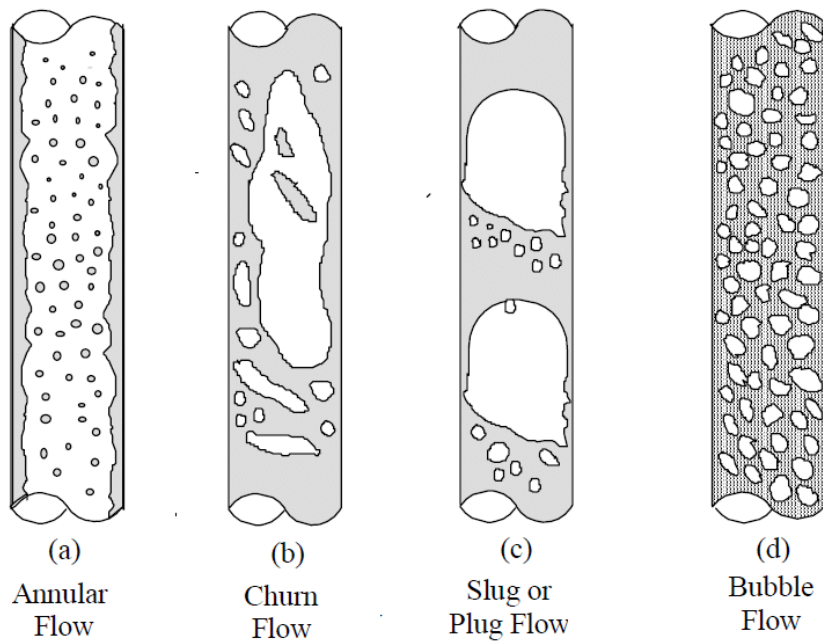


Figure 2.5: Different flow regimes, figure from [18].

2.3. Literature review on Reservoirs

While, in theory, a wide range of reservoirs could be used, in this report, we focus on the two types most likely to be used for CCS. These two types are saline aquifers and (depleted) gas fields. In this section, we outline what characterizes these reservoirs and shortly look at research and experience that has been done.

2.3.1. Saline Aquifers

Saline aquifers are a popular target for CCS as it has the largest storage potential and are present globally [11]. In the last decades, industry has already developed experience with this reservoir for CCS purposes. Projects like Slepner, and Snovit en In Salah bring much-valued multi-year experience [20] lacking in other types of reservoirs. Experience with CCS does however not carry over one-to-one to CPG. Which has its own challenges to overcome.

Literature study

CPG in aquifers is by far the most widely studied application. Norouzi et al. studied the performance in fluvial aquifers and determined the optimal well spacing and injection rate for such reservoirs [45]. Another study by Xu et al. investigated how heterogeneity affected performance [68]. [54] show that CPG could make CCS much more economically feasible [54]. Another concept being developed is the use of CPG as a flexible energy source and/or earth battery [26].

A major hurdle for CPG in Aquifers is what has recently been referred to as the "Plume Establishment" (PE) stage. During initial injection, thermosiphon-driven convection is not possible, and only water will be produced. If the production well is shut in, the pressure will rise. During this stage, no electricity production will be possible, and a considerable amount of energy needs to be invested in the system.

Plume Establishment

The PE stage brings about two main problems. First, "fresh" CO_2 needs to be brought into the system and from the ambient state into the approach state, which is an energy-intensive process. This CO_2 needs to be compressed by at least 50 bar to the liquid state for it to be ready for injection.

Secondly, if the production wells are not shut in during this stage, copious amounts of water will be produced, and how this should be disposed of is not yet agreed upon. Some studies suggest a solution as simple as releasing it into the ocean could be a viable method of disposal and might have limited

environmental effects [19]. The more expensive option of re-injection, as is done i.e. for the Gorgon project [13], might be the only possible and legal option in other cases.

As the PE stage could take 10+ years before the reservoir is ready to start production [23], this strongly influences a reservoir's suitability for CPG. This is the case especially when energy production is of primary importance, such as a sub-sea powerplant [37], and a CCS phase is not directly connected.

2.3.2. (Depleted) Gasfields

Depleted gas fields are another possible target for CPG. While Saline Aquifers have been used more for CCS, CO_2 injection in depleted gas fields is not a new concept. As mentioned by "Carbon Dioxide Capture and Storage (CCS) in Saline Aquifers versus Depleted Gas Fields" Projects like re-injection at the K-12 B field, and the Otway and Rouse pilot have been going for a long time. For CCS purposes gasfields appear to have some clear benefits such as; Pre-existing infrastructure, a high amount of available pore space and fewer geomechanical risks. Risks like hydrate formation due to JT cooling cause CO_2 injection into depleted Gasfields to be perceived as more uncertain as saline aquifers.

Literature study

While less studied than aquifers, several studies have proposed coupling CPG with natural gas recovery. As an extension of enhanced gas recovery (EGR) it could help increase the recovery factor [71] [16] [24]. CPG could play a role as a novel method to recover additional natural gas hydrates [38]. Furthermore, in contrast to aquifers, claims have been made that a thermosiphon has been successfully established [8].

Plume establishment time

A major advantage gas fields have over aquifers is that it is not necessary to produce water until you get a breakthrough, but they can constantly produce gases that do not need to be disposed of. Re-pressurising the reservoir in between the end of the EGR stage and geothermal production could be necessary and function as the PE stage [45]. The stages for a gasfield are shown in figure 2.6.

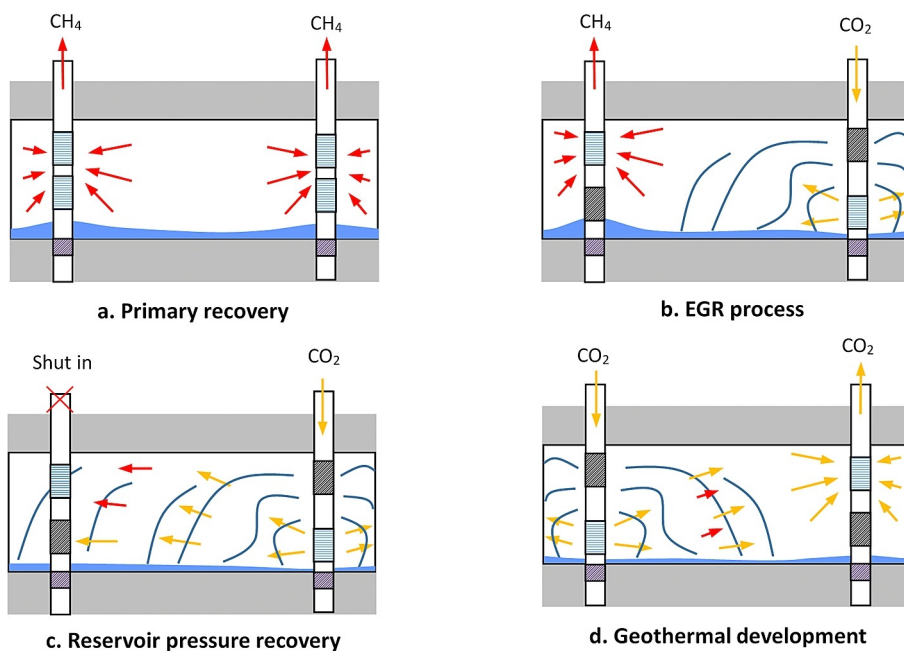


Figure 2.6: The four phases of the lifecycle of CPG in a gasfield from [16].

3

Methodology

For this work, we build a model for a CPG system. In such a system many different elements need to be considered. When injecting CO_2 into a reservoir, many different processes of different origins come into play. Thus, a reservoir simulator capable of capturing thermal multiphase flow behaviour is required. Other parts of the cycle, the wellbore, turbine, and condenser, should also be considered to get an estimate of the electricity produced by the system. In the upcoming sections, we will describe our methodology for each of these elements. We will start with how our reservoir model is constructed, and then we continue with the description of our simulation model, and its properties. Lastly, we will include an elaborate on the rest of the cycle and which simplification we use.

3.1. Reservoir model

3.1.1. Gridding

For our reservoir setup, we utilise cartesian gridding, dividing the reservoir into rectangular cells. Structured grids induce a directional preference, which can introduce errors if the projected geology's anisotropy doesn't match the orientation. For this study, we generally use homogenous reservoir models lacking complex geological features; thus we do not suffer from these problems. Opting for a cartesian grid also provides us with faster grid generation. Additionally, its K-orthogonality allows us to employ a two-point flux approximation instead of a multi-point flux approximation, which is significantly faster.

3.1.2. Component selection

In (depleted) hydrocarbon reservoirs, many different components can be present; gas reservoirs i.e. may contain H_2O , CO_2 , C_1 , C_2 , C_3 , C_4 , N_2 , H_2S and other trace components [16]. For our purposes, we will try to limit the number of components in our simulation, as every additional component increases the degrees of freedom of our state and greatly impacts our computational speed. We will consider two types of reservoirs, each with its own amount of components. Two components (H_2O , CO_2) for an aquifer, three components (H_2O , CO_2 , C_1) for a gasfield.

3.2. Multiphase-flow through porous media

As we compare several reservoirs with several components and phases in this study, . We need to model the following processes:

- Multiphase-flow through porous media.
- Heat conduction and convection through porous media
- The thermodynamical partition and properties of all phases.

Here, we follow a similar approach as in literature [48], We consider the mass balance for an arbitrary

volume as given by equation 3.1.

$$\int_D \frac{\partial}{\partial t} \phi \rho dV + \oint_S (\rho \vec{u}) \vec{n} dA + \int_D \dot{q} \rho dV = 0 \quad (3.1)$$

Where ϕ is the porosity, ρ the density of the fluid, \vec{u} the volume flux, and the total flux \dot{q} the source/sink term.

Using Gauss's theorem we can rewrite the middle term and take out the integrals, we yield equation 3.2.

$$\frac{\partial}{\partial t} (\phi \rho) + \nabla \cdot (\rho \vec{u}) + \dot{q} \rho = 0 \quad (3.2)$$

While this equation holds, it does not discriminate between phases, we decompose it by component and phase before we solve. We split up for every phase j and define for every component c . We obtain a set of equations 3.3 equal in number to the amount of components.

$$\frac{\partial}{\partial t} (\phi \sum_j x_{cj} \rho_j s_j) + \nabla \cdot (\sum_j x_{cj} \rho_j \vec{u}_j) + \sum_j x_{cj} \rho_j \dot{q}_j = 0, \quad c = 1, \dots, n_c. \quad (3.3)$$

We assume Darcy-flow in a gravitational field. We neglect diffusion and dispersion effects as these are generally negligible in our conditions. The volume flux per phase \vec{u}_j is given by equation 3.4.

$$\vec{u}_j = -\frac{k k_{rj}}{\mu_j} (\nabla P_j + \rho_j \vec{g}) \quad (3.4)$$

There exists a pressure difference between each phase, which is possible because of interfacial surfaces and can be determined by capillary pressure functions as shown in equation 3.5.

$$P_j - P_k = P_{ckj}, \quad j = 1, n_p, k = i, n_p, k \neq j \quad (3.5)$$

Where P_{ckj} denotes the capillary pressure between the phases k and j . P_{ckj} is a function of the saturation. We will neglect these effects.

Porosity, ϕ , is taken to be linearly dependent on the pressure as given in equation 3.6.

$$\phi = (1 + c_r(p - p_{ref})) \phi_0 \quad (3.6)$$

3.2.1. Heat conduction and convection through porous media

A similar approach can be taken for an energy balance [65]. Here, we only look at heat transfer and neglect other forms of energy transfer, such as momentum, as this is already implicitly included in Darcy's law. The full balance is given by equation 3.7.

$$\frac{\partial}{\partial t} (\phi \sum_{p=1}^{n_p} \rho_p s_p U_p + (1 - \phi) U_r) - \nabla \cdot \sum_{p=1}^{n_p} h_p \rho_p u_p + \nabla \cdot (\kappa \nabla T) + \sum_{p=1}^{n_p} h_p \rho_p \dot{q}_s = 0 \quad (3.7)$$

3.2.2. Thermodynamics

In this work we follow the approaches as established in *Thermodynamic Models: Fundamentals and Computational Aspects*. For mixtures of multiple components forming multiple phases we can assume there to be chemical equilibrium (equation 3.8)

$$\mu_{ij} = \mu_{ik}, \quad i = 1, \dots, n_c, j = 1, \dots, n_p, k = 1, \dots, n_p, k \neq j \quad (3.8)$$

or equivalently equal partial fugacities (equation 3.9)

$$\hat{f}_{ij} = \hat{f}_{ik}, \quad i = 1, \dots, n_c, j = 1, \dots, n_p, k = 1, \dots, n_p, k \neq j \quad (3.9)$$

Additionally, the mole fractions should sum to one for each phase (equation: 3.10).

$$\sum_{c=1}^{n_c} (x_{cj} - x_{ck}) = 0, \quad j = 1, \dots, n_p, k = 1, \dots, n_p, k \neq j \quad (3.10)$$

Equivalently for the saturation

$$\sum_{j=1}^{n_p} S_j = 1 \quad (3.11)$$

and lastly for the composition holds equation 3.12.

$$z_c - \sum_{j=1}^{n_p-1} L_j x_{cj} = 0, \quad c = 1, \dots, n_c \quad (3.12)$$

Equation 3.9 yields us $n_c(n_p - 1)$ equations, 3.12 yields us n_c equations and 3.10 ($n_p - 1$) equations. Summing up to $n_c(n_p) + (n_p - 1)$ equations. As unknowns we have $P, T, \mathbf{x}_{cp}, L_p$ which give us $n_p(n_c + 1) + 1$ unknowns. This leaves us with an underdetermined system with a rank deficiency of 2.

Tangent Plane

Every system constantly drifts to maximise its entropy under the constraint of constant energy. The Gibbs Free Energy (μ) can determine the effective balance between these two forces (equation 3.13). Its minima give us the stable states of the system.

$$G = H - TS \quad (3.13)$$

For a phase to be stable, changing the composition from w to any other composition z , the change in Gibbs Free Energy should be positive. Equivalently equation 3.14 states the tangent plane condition.

$$\sum_{i=1}^C w_i (\mu_i(\mathbf{w}) - \mu_i(\mathbf{z})) > 0 \quad (3.14)$$

Additionally, as stated in equation 3.8, all phases must have equal chemical potential and thus the tangent to this plane will be equal for both phases.

Negative flash

A second approach is to introduce so-called equilibrium factors. We describe the equilibrium (K-value) of a two-phase system is defined as given in equation 3.15 [58].

$$K_i = \frac{x_{i1}}{x_{i2}} = \frac{\hat{\phi}_{i2}}{\hat{\phi}_{i1}} \quad i = 1, \dots, n_c \quad (3.15)$$

Where $\hat{\phi}_{ij}$ is the non dimensional fugacity coefficient relating the effective pressure to the deviation from ideal gas and is equal to:

$$\hat{\phi}_{ij} = \frac{f_{ij}}{x_{ij}P}, \quad i = 1, \dots, n_c \quad (3.16)$$

The initial guess for the K-values is generally found using the Wilson equation 3.17.

$$K_i = \frac{x_{i1}}{x_{i2}} = \frac{P_{ci}}{P} \exp \left\{ 5.37 (1 + \omega_i) \left(1 - \frac{T_{ci}}{T} \right) \right\} \quad (3.17)$$

Here, we continue with the equations as derived in *Thermodynamic Models: Fundamentals & Computational Aspects* [39].

$$\sum_{i=1}^{n_c} z_i \frac{K_{ij} - 1}{1 + \sum_{l=1}^{n_p-1} L_l (K_{il} - 1)} = 0, \quad j = 1, \dots, n_p - 1 \quad (3.18)$$

Equation 3.18 is then solved in DARTS-flash as outlined by Wapperom et al. [66] by using convex transformations as proposed by Nichita and Leibovici [41]. Furthermore the equation of state can be determined using the Peng Robinson (PR) equation.

3.2.3. Properties

Most of our properties in this work are calculated through the open-source DARTS-flash library [47]. The rest are from the open-DARTS standard library of relations. We will not go depth for these relations in this report, but the relations are summarised in table 3.1.

Property	Relation
Density (Vapour phase) ρ_V	EoS
Density (Aqueous phase) ρ_{Aq}	Garcia (2001)
Viscosity μ_V	Fenghour, Wakeham & Vesovic (1998)
Viscosity μ_{Aq}	Akand W. Islam & Eric S. Carlson (2012)
Relative permeability k_r	Brooks-Corey
Enthalpy H_V	EoS
Enthalpy H_{Aq}	EoS
EoS (Vapour phase)	Peng-Robinson
EoS (Aqueous phase)	Ziabakhsh-Ganji and Kooi

Table 3.1: Table with relationships used in the reservoir simulation. EoS indicates that the property is derived from the corresponding Equation of State.

Phases

Within a two-component system like H_2O-CO_2 , seven possible phase combinations could theoretically develop as displayed in figure 3.1. As the figure shows, we have three distinct phases: Aqueous (a), Liquid (l) and a vapour phase (g). We expect no liquid carbon to present within the domain of reservoir states, as shown in figure 3.2. This allows us to take a two-phase approach where we only consider a H_2O rich aqueous phase and a CO_2 rich vapour phase. We neglect salt presence. For modelling the phases, DARTS-Flash takes an approach very similar to that of Jager, Ballard, and Sloan Jr [35]. This study proposes a method that describes the aqueous phase fugacity more accurately than the usual EOS used for hydrocarbons. It introduces a modified Helgeson EOS [59] that is valid for water-dominated aqueous phases with a molar composition of > 0.65 and a validity of up to 5000 bar.

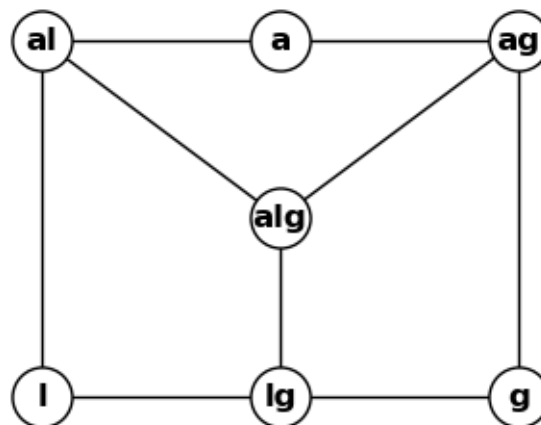


Figure 3.1: Seven phase combinations, as [49].

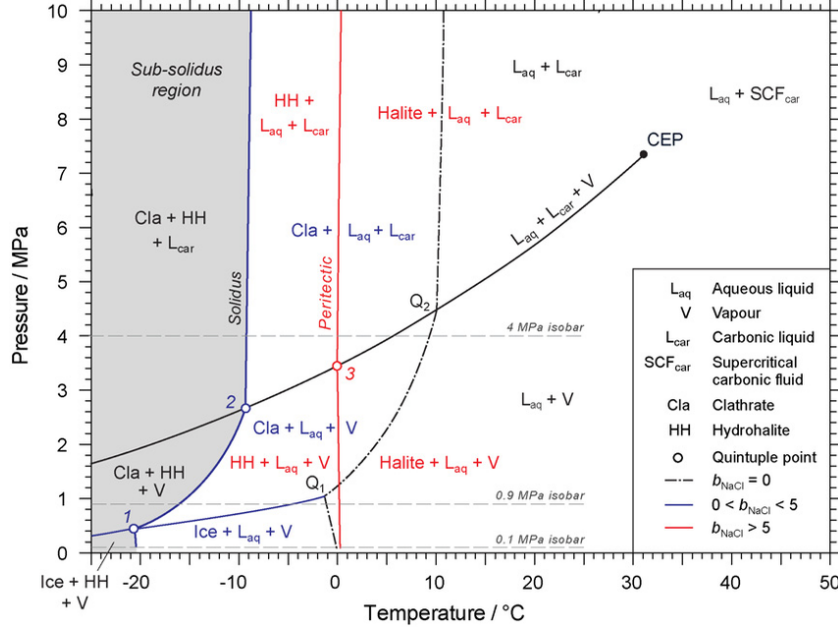


Figure 3.2: Stable phase relations in a CO₂-H₂O-NaCl system, from [4].

Aqueous phase

Continuing following the approach taken by Jager, Ballard, and Sloan Jr, We model the solute and water using different EoS. The aforementioned Helgeson EoS is used to calculate the pure water state. Then, a second EOS is used to calculate the deviation from this ideal state. Here we diverge from [35] and use the EoS developed by Ziaabakhsh-Ganji and Kooi. This EoS allows for accurate modelling of brine and gas mixtures. It can be used for a wide range of pressures (up to 600 bar) and temperatures (5° C - 110° C). Another benefit of this EoS is that it can be solved non-iteratively since it neglects interactions between gasses.

Vapour phase

The PR EoS is used for the vapour phase. This EoS has been used for a long time for hydrocarbons and is the industry standard. We use this EoS to describe the CO₂ rich vapour phase with H₂O dissolved. While we will mostly use it for the vapour phase, this EoS is also capable of describing the CO₂ mixtures at liquid state, which is useful for injection applications. The relevant equations are given below.

$$P = \frac{RT}{v-b} - \frac{a\alpha}{v(v+b) + b(v-b)} \quad (3.19)$$

$$a = 0.45724 \frac{R^2 T_c^2}{P_c} \quad (3.20)$$

$$b = 0.07780 \frac{RT_c}{P_c} \quad (3.21)$$

$$\alpha = 1 + \kappa(1 - \sqrt{T_r})^2 \quad (3.22)$$

$$\kappa = 0.37464 + 1.54226\omega - 0.26992\omega^2 \quad (3.23)$$

$$A = \frac{\alpha a P}{R^2 T^2} \quad (3.24)$$

$$B = \frac{b P}{RT} \quad (3.25)$$

$$Z^3 - (1-B)Z^2 + (A-2B-3B^2)Z - (AB-B^2-B^3) = 0 \quad (3.26)$$

Where $T_r = \frac{T}{T_c}$, T_c the critical temperature, P_c the critical pressure, v the volume, Z the compressibility, and the ω the acentric factor.

3.3. Thermodynamic Cycle

In this work, we evaluate the performance of a reservoir based on, among other things, the net amount of energy produced. As CPG is a system in a loop, every state in the cycle determines the rest of the system. We thus need to calculate the entire cycle to acquire a proper estimation of electrical energy produced by the system.

3.3.1. Modelling Isentropic processes

The turbine within our simulation thermodynamic processes can be approximated as an isentropic process. We use this assumption to determine the temperature after the turbine within the thermodynamic cycle, as shown in figure 3.3. Δs_{ideal} (entropy change per mole) for an ideal gas is defined as in equation 3.27.

$$\Delta s_{ideal} = \int_{T_1}^{T_2} \frac{C_P(T)}{T} dT - R \int_{P_1}^{P_2} \frac{1}{P} dP \quad (3.27)$$

Where T is the temperature, P is the pressure, and C_p is the heat capacity under constant pressure.

We can determine C_P , heat capacity under constant pressure (per mole), for an ideal gas using a polynomial of the 3rd order using equation 3.28, with the component-specific parameters [35].

$$C_P(T) = aT^3 + bT^2 + cT + d \quad (3.28)$$

Using the concept of residual functions, we know that entropy per mole (s) equals.

$$s = s_{ideal} + s_{residual} \quad (3.29)$$

In which the residual function for entropy can be determined through rewriting equation 3.13.

$$s_{residual} = \frac{g_{residual} + h_{residual}}{T} \quad (3.30)$$

Where $g_{residual}$ is the Gibbs free energy per mole and $h_{residual}$ is the residual enthalpy per mole. So, for an isentropic process holds:

$$0 = \Delta s = \Delta s_{ideal} + \Delta s_{residual} \quad (3.31)$$

Under this constraint and using equations 3.27 and 3.10, we can solve problems with a single unknown. As for the turbine, where the outlet temperature is the only unknown, we can solve this numerically with the bisection method.

3.3.2. Cycle components

In this work, we consider an idealized cycle with a single turbine and a condenser, as shown in figure 3.3. In the upcoming section, we will explain the simplifications we used for the several steps in the cycle.

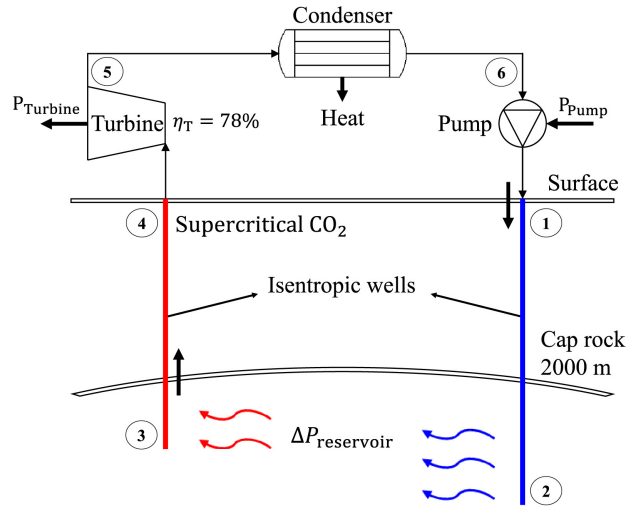


Figure 3.3: A direct use thermodynamic cycle for CPG from [45].

3.3.3. Wellhead to bottom hole (State 1 to 2)

The state at the wellhead (state 1) is the only state in the cycle we directly control. From the wellhead, the CO_2 travels to the bottom-hole state (state 2); for this simple case, we start by defining an energy balance for the wellbore where we follow Sun et al. [61]. This gives us a balance for a single-phase fluid in equation 3.32.

$$\frac{dQ}{dL} = C_p \frac{dT}{dL} - C_p C_j \frac{dp}{dL} - g \sin \theta + v \frac{dv}{dL} \quad (3.32)$$

We simplify this equation by assuming we have perfect vertical wells and neglect heat dissipation through the pipes and momentum losses. We get equation 3.33.

$$\frac{dT}{dL} = C_j \frac{dp}{dL} + \frac{g}{C_p} \quad (3.33)$$

Assuming $\frac{dp}{dL}$ to be the hydraulic pressure. For the annular flow regime we can assume the liquid hold-up in the gas core to be zero. Furthermore, we neglect interfacial stresses we follow [9] where we define $\frac{dp}{dL}$ as in equation 3.34.

$$\frac{dp}{dL} = \rho_g \alpha g + \rho_l (1 - \alpha) g \quad (3.34)$$

Where ρ_g is the density of the gas phase, ρ_l is the density of the liquid phase, α is the volume fraction of the gas phase, and g is the gravitational acceleration. As for the injection well, the wellhead state is constant; we consider the bottomhole state constant as well. The production well does need to be continuously evaluated as the inlet state changes.

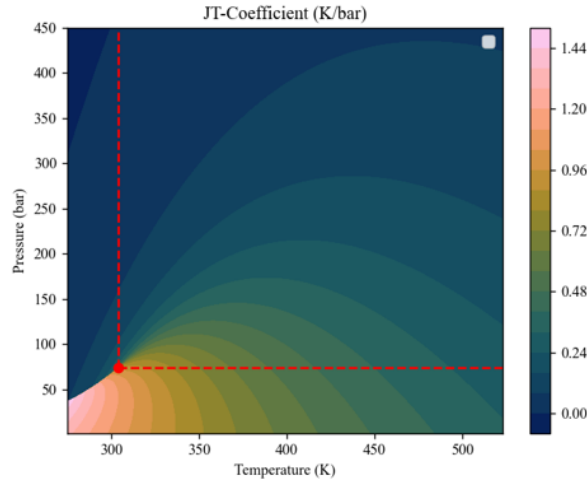


Figure 3.4: Joule-Thompson coefficient for pure CO_2 .

3.3.4. Reservoir (State 2 to 3)

During this step, the actual reservoir simulation will be done using open-DARTS [63]. The equations and relations explained in previous sections are used.

3.3.5. Bottom hole to wellhead (State 3 to 4)

This process is similar to the injection well shifted in temperature and pressure. The CO_2 is now in supercritical phase instead of the liquid phase. Giving it a much more pronounced Joule-Thompson Coefficient. Under isenthalpic conditions the temperature is thus much more dependent on the pressure and significant cooling happens while the CO_2 travels upward the borehole.

3.3.6. Turbine (State 4 to 5)

The turbine is treated as an isentropic process with an isentropic efficiency of 78%, as is done in many similar studies [25][45][2]. Where the isentropic efficiency is defined by equation 3.35. h_{in} is the molar enthalpy of the fluid entering the turbine, $h_{out,isentropic}$ the molar enthalpy after the turbine if treating the process as isentropic, and h_{out} the real outgoing molar enthalpy.

$$\eta_{turbine} = \frac{h_{in} - h_{out}}{h_{in} - h_{out,isentropic}} \quad (3.35)$$

Within the turbine, the sCO_2 will expand to the vapour phase and most of the energy will be converted to work. Because of the non-ideal isentropic efficiency, more energy is lost due to diabatic processes. The amount of electric power generated by the turbine can then be calculated as equation 3.36

$$P_{turbine} = h_{in} - h_{out} \quad (3.36)$$

3.3.7. Condenser

After the turbine, the CO_2 is condensed back to the approach state 1. The energy produced is equivalent to the enthalpy difference between the outlet state of the turbine and the injection/approach state. While in practice, this process is non-ideal and has a certain efficiency (λ), we neglect this and take $\lambda = 1$ as the losses are highly dependent on the specific set-up of the surface infrastructure.

$$P_{Condenser} = \lambda(h_{in} - h_{out}) \quad (3.37)$$

3.4. Cycle evaluation

By completing our set of equations, we can evaluate the state over the entire cycle. Several properties of the entire cycle are shown in figures 3.5, 3.6, and 3.7.

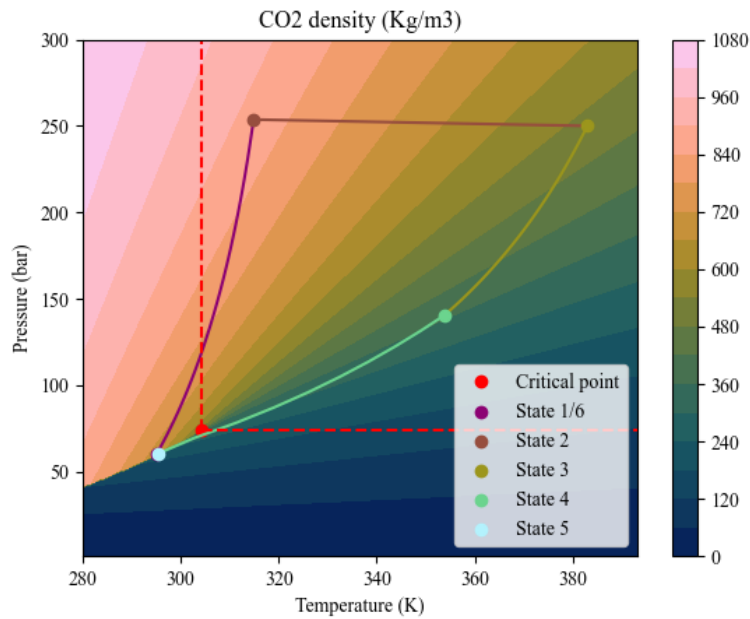


Figure 3.5: The thermodynamic path for the entire cycle overlaid over the density of CO_2 . Pure CO_2 is assumed here.

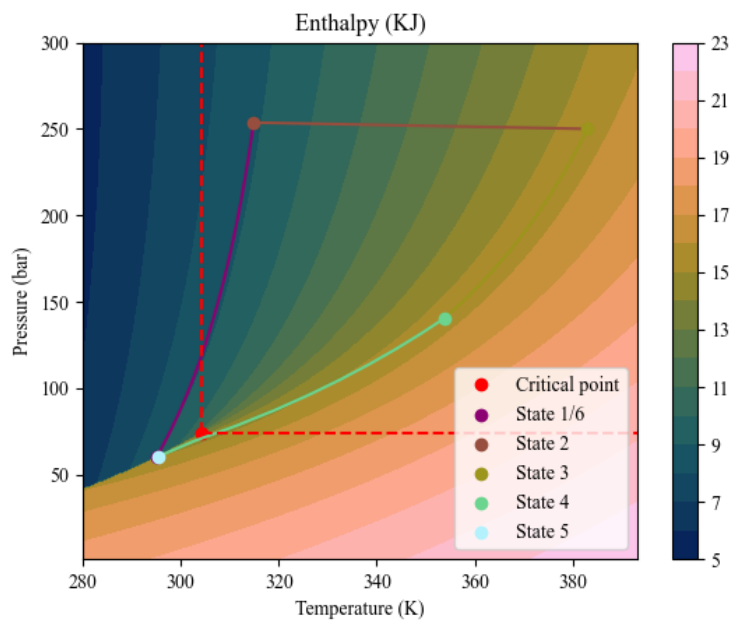


Figure 3.6: The thermodynamic path for the entire cycle overlaid over the density of CO_2 . Pure CO_2 is assumed here.

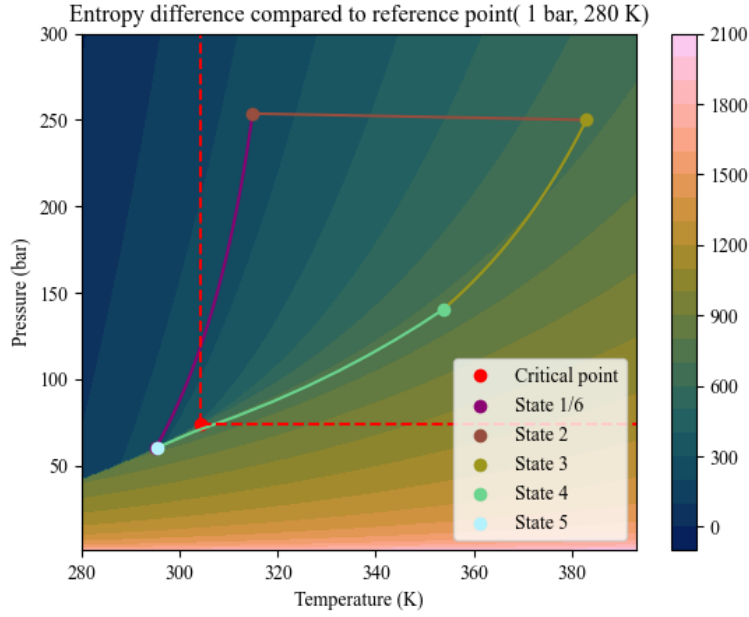


Figure 3.7: The thermodynamic path for the entire cycle overlaid over the entropy of CO_2 . Pure CO_2 is assumed here.

3.5. Operator Based Linearization

What distinguishes Open-DARTS from many other simulators is the implementation of operator-based linearization (OBL) as presented in [64], and extended to the thermal case in [65]. OBL allows for the governing equation of our finite-volume approach to be treated as a combination of operators. These operators are fully determined by the independent $2 + (n_c - 1)$ variables, $(P, T, z_1 \dots z_{n_c-1})$. These variables uniquely define our state (ω). Where we take N evenly spaced supporting points in $\Omega \subset \mathbb{R}^{n_c+1}$ [36], with Ω given by equation 3.38.

$$\Omega = \{x_1, \dots, x_{n_c+1} \mid x_i \in I_i\} \text{ With } I_i = [a_i, b_i] \text{ for } i = 1, 2 \text{ and } I_i = [0, 1] \text{ for } i = 3, \dots, n_c + 1 \quad (3.38)$$

While the choice of $[a_i, b_i]$ is essentially arbitrary, take $[a_1, b_1] = [1, 400]$ bar and $[a_2, b_2] = [273.15, 393.15]$ K .

For these supporting points, we now calculate relevant operators dynamically.

3.5.1. Operator Expansion

As shown in the previous sections, when evaluating CPG it's important to study the entire cycle. The path of our system in state space is shown in figure 3.6. Within this figure, we have taken Ω as the boundaries of this plot. Thus, We can clearly see $\Omega_{cycle} \subset \Omega$. This allows us to use the exact same supporting points for both the operators in the reservoir, within the well, and on the surface. Using the production data from our reservoir simulation we choose to extend this framework to evaluate the well and then the turbine. In figures 3.8 and 3.9, the wellhead states determined using OBL versus generic solution are plotted.

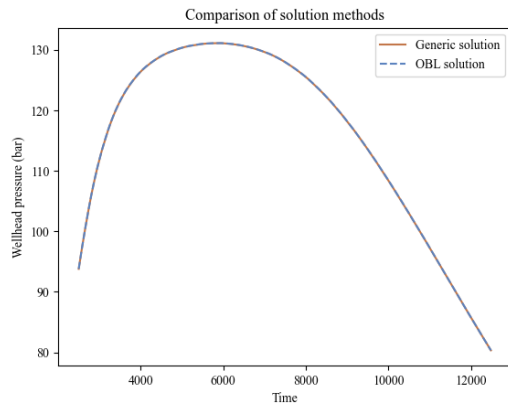


Figure 3.8: Wellhead pressure of a typical production profile.

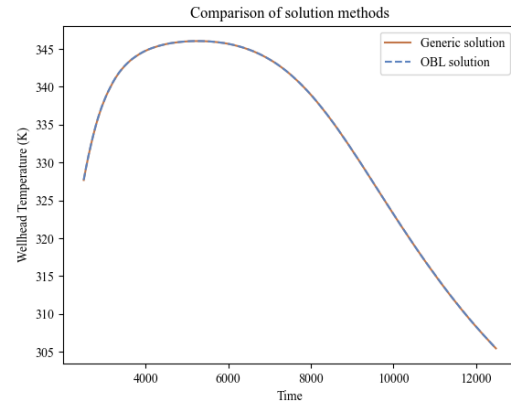


Figure 3.9: Wellhead temperature of a typical production profile.

In practice, we are not interested in the wellhead state and don't construct an operator for this. We are only interested in how much electrical energy our turbine generates. We evaluate the turbine using the concept of isentropic efficiency as shown in figure 3.10. We also add an operator for the heat extracted by the condenser. An comparison between the generic method of calculating the energy and the OBL method is shown in figure 3.11.

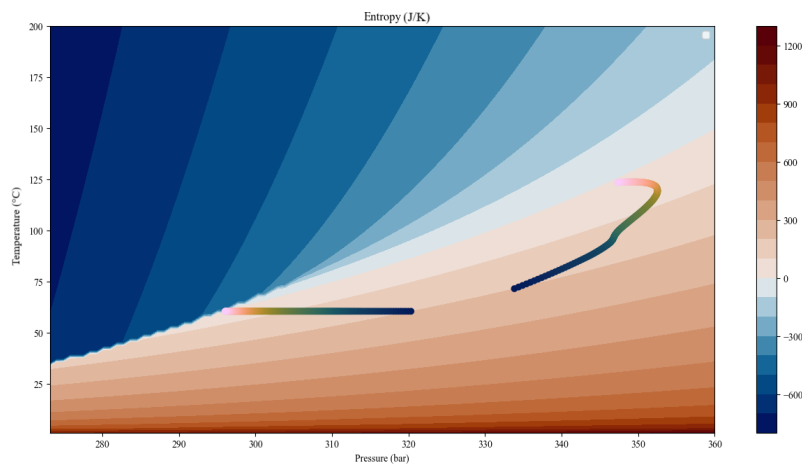


Figure 3.10: States in and out of the turbine for a typical production pattern. Pairs have the same colour. We have taken the isentropic efficiency to be 1 for illustrative purposes.

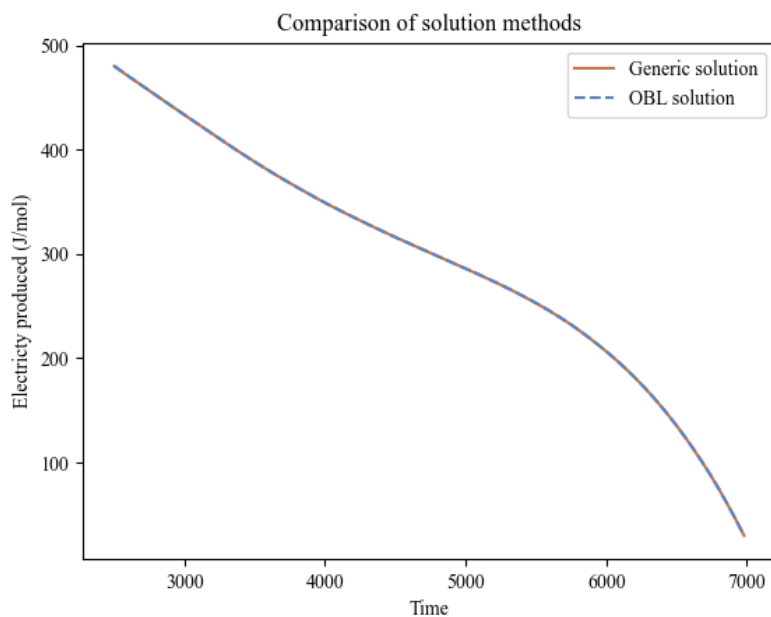
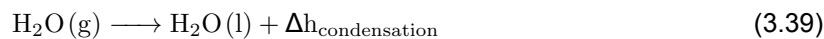


Figure 3.11: Turbine energy output for both direct calculation and OBL calculation.

We find that for 100 supporting points, the OBL approach matches direct calculation extremely well.

3.6. Phase transitions

During the phase transition of a pure component, the enthalpy will change but the temperature will remain constant. For water, this is displayed in figure 3.12. This process equation (3.39) is exothermic and releases energy. For a mixture of gases, this discontinuity will smooth out, making the enthalpy a proper function with a binary relation of its pressure-temperature state.



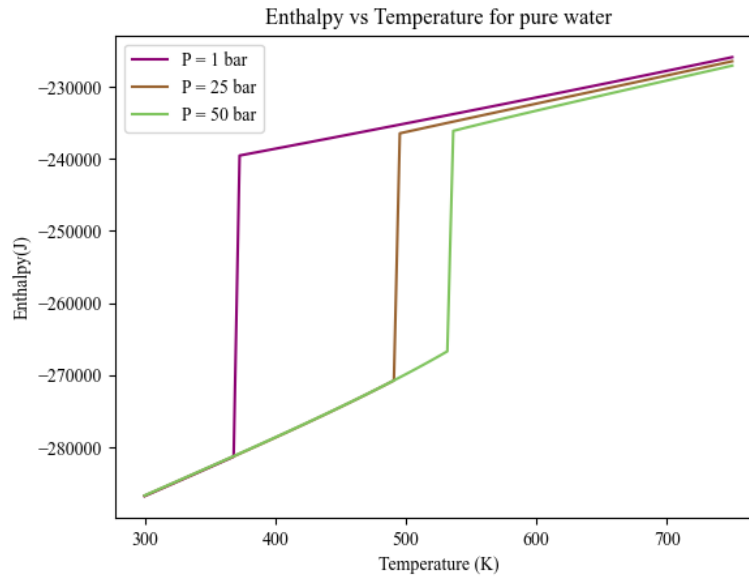


Figure 3.12: Enthalpy

Fleming et al. [27] showed that the exsolution of water from the vapour phase to the aqueous phase in the wellbore strongly influences its wellhead temperature. During the expansion of the gas in the turbine, this dissolution will happen as well. In our model, we will include these effects for the zero-dimensional turbine model for the aquifer, while omitting them for the well model due to implementation challenges.

3.7. Parameters

Well spacing/ Reservoir length

In a system where the convection is purely driven by the thermosiphon the control over the pressure differential between the wells is limited. While the injection could be altered, there is generally a clear optimum. One way to directly influence the pressure gradient within the reservoir is to alter the well spacing. And thus well spacing has been shown to be a significant factor for reservoir performance for CPG [40][43]. Previous studies have found a value of around 500 meters to be optimal, this is also the distance used in several studies [45] [22] [24]. As well spacing is not a research question of this study, we will use this value too.

Wellhead state

The state just before injection is the only state we can directly set and influences the entire cycle. The wellhead injection state directly influences the system in three ways: the bottom hole state, the energy generated by the turbine, and the energy required to bring new CO_2 into the system. We set our injection state assuming an average surface temperature of $15^\circ C$ and an approach temperature of $7^\circ C$ with a pressure of 0.5 bar above the condensation pressure for this temperature, 57.8 bar. This has been suggested as the optimal injection state for this reservoir type [2].

3.8. Performance metrics

To determine the performance of different types and environments, we must decide on widely applicable performance metrics that quantify performance and allow us to compare quantitatively. A natural approach is to construct several performance metrics.

CO_2 Replacement Ratio

We define the CO_2 Replacement Ratio as the ratio between the injected and produced CO_2 . This is an important measurement as it quantifies how much CO_2 is used for heat extraction and how much

needs to be added to the system. We can define this instantaneously (equation 3.40), and its integral would give us a metric for the whole period of operation (equation 3.41).

$$RR(t) = \frac{Q_{Production,CO_2}(t)}{Q_{Injection,CO_2}(t)} \quad (3.40)$$

$$RR_{CO_2,total} = \int_0^{T_{End}} \frac{RR(t)}{T_{End}} dt \quad (3.41)$$

Electrical energy generated

The most crucial characteristic of CPG is the amount of electricity that can be produced (MWe). This allows for comparison with other renewable technologies, such as conventional geothermal, solar, and wind. This metric will quantify simply the amount of energy produced and can be calculated by equation 3.42. In this equation $Q_{Production,V}$ denotes the amount of vapour phase produced daily.

$$P_{turbine} = (h_{in} - h_{out})Q_{Production,V}(t) \quad (3.42)$$

The heat the condenser produces can then be calculated by the remaining enthalpy. This is equivalent to the difference in enthalpy between the turbine outlet state, h_{out} , and the enthalpy at the injection wellhead, h_{inj} .

$$P_{condenser} = Q_{Production,V}(t)(h_{out} - h_{inj}) \quad (3.43)$$

Water Fraction

During operation a significant watercut will be produced. The problem of what to do with this produced water is not trivial and has not been solved. Releasing it in hydrodynamically active regions like the North Sea appears to have a limited impact on the environment [19]. This will not be an option everywhere, and the exact environmental impact and legality is not yet understood. Furthermore, as on-shore storage is considered infeasible, re-injection may be the only option for disposal. This is a whole problem on its own and may severely impact the profitability of the entire operation. Therefore, we introduce another performance metric, the molar amount of water produced.

3.9. Gains from our method

Computational efficiency

The Open-DARTS framework's strength lies in the modelling of highly nonlinear physics with operator-based linearization, which ensures high computational performance. Given its highly customisable and open-source, we show to extend these strengths to the entire cycle required for the modelling of CPG performance. A previous study was done on CPG using the open-DARTS framework, then named DARTS, that neglected any part outside of the reservoir. We include the entire cycle to capture essential and CPG characteristic effects such as the thermosiphon. Additionally, this allows us to calculate electricity produced directly and more accurately predict the end of life for the reservoir. A direct benefit of our approach is the much increased computational efficiency of our methods. While performance metrics for other studies do not exist, the sparsity of data points in other studies regarding electricity production does imply a computational bottleneck. In our fully coupled and integrated approach, we yield these values for every data point, giving us a high data resolution.

DARTS-Flash

In many of the recent studies modelling the surface infrastructure, the CoolProp library has arisen as the de facto standard library [43] [22] [57] [29]. In this study, we deviate from this approach and utilize the DARTS-Flash library.

CoolProp reports a point simulation time of around $5 * 10^{-5}$ seconds [6]. Our tests with the Python wrapper on our local hardware found similar values for the lower-level abstract library and with the standard propsSI library being severely slower. In our comparison, 10^4 points are calculated for each property where the average elapsed time is plotted in figure 3.13.

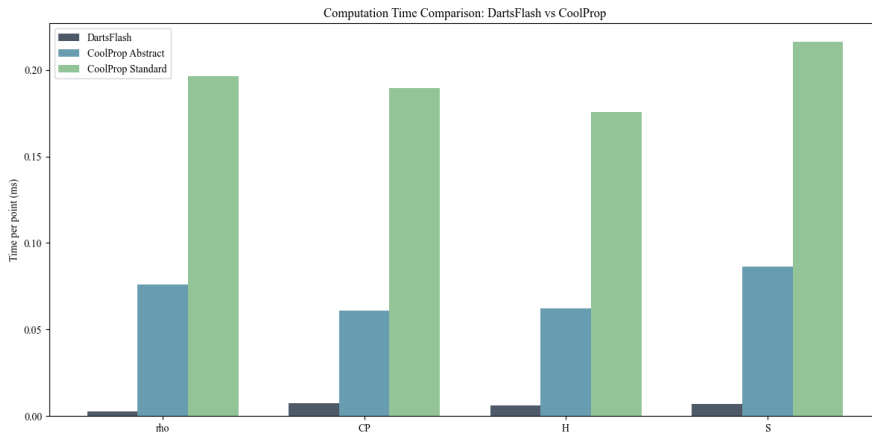


Figure 3.13: Average elapsed time for various thermodynamic properties. Rho represents density, CP heat capacity, H enthalpy, and S entropy.

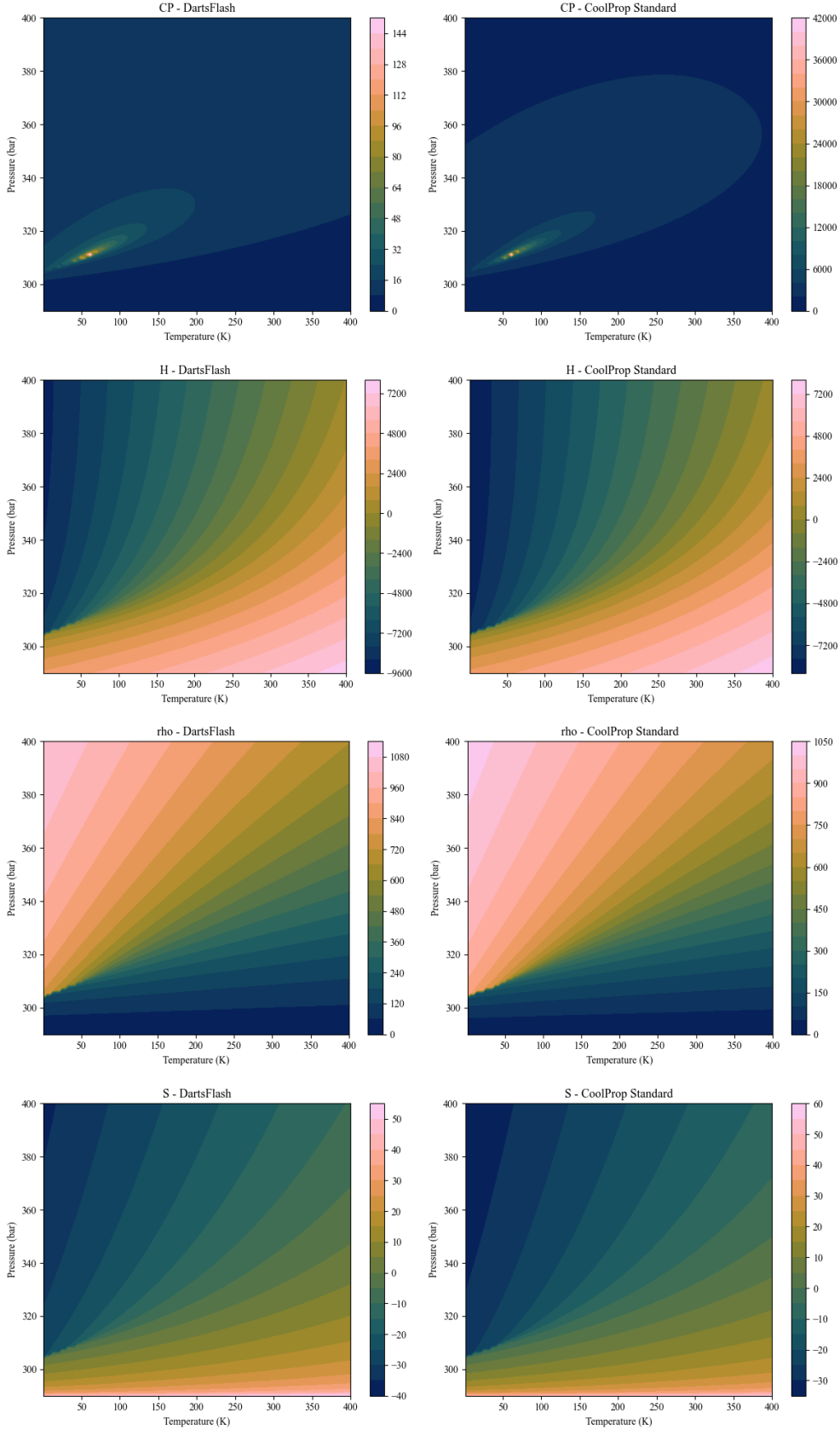


Figure 3.14: Several values plotted for DARTS-Flash. Rho represents density, CP heat capacity, H enthalpy, and S entropy.

As described earlier, a multi-phase multi-component approach is required to model the reservoir, but it also affects the in the surface infrastructure. CoolProp has flash capabilities but these are generally considered limited or unstable and rely on binary pairs. Given our multi-component environment, such as the gasfield, where the vapour phases consist of three components, a multi-component approach is required.

Multi-component approach

Our robust multi-component approach comes most visibly to fruition in our turbine evaluation. As for isentropic evaluation in the turbine, we follow an isentrope to our output pressure to find our output temperature. These isentropes are very dependent on the mixture as can be seen in figure 3.15.

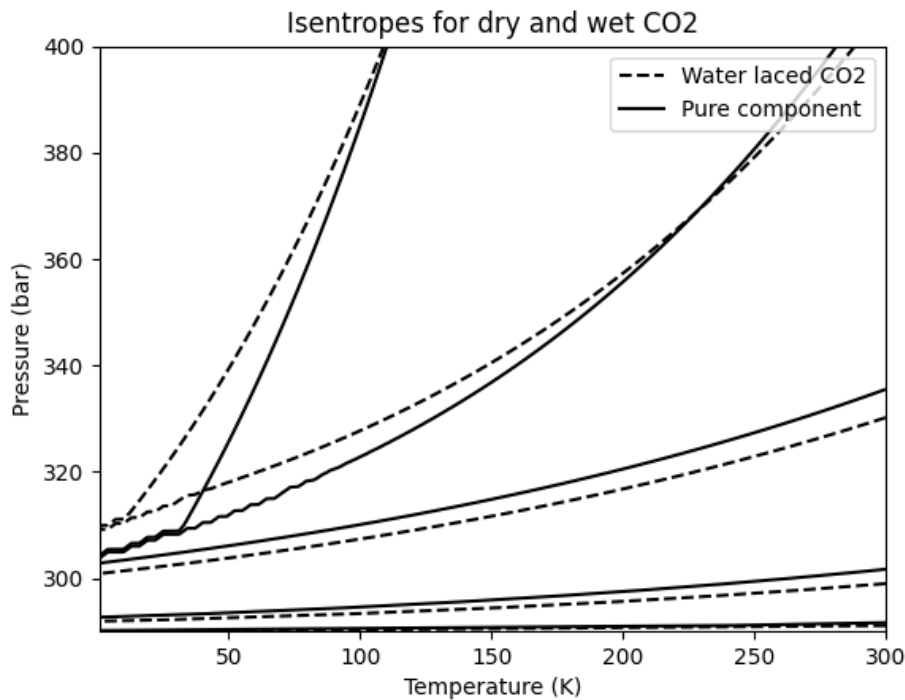


Figure 3.15: Isentropes for H_2O-CO_2 mixture.

Control by electricity production

Using a fully coupled and efficient model, we can determine the electricity produced for every step "on the fly" with negligible performance impact. This opens up many possibilities for interaction between the surface machinery and the reservoir control. We can now control by electricity production and aim for a steady electricity rate. Additionally, As CPG is often proposed to be an on-demand-based system providing electricity at times where i.e. weather based sources cannot. We can now also model a seasonal electricity production.

4

Verification

To verify our model, we consult Ezekiel's work. In his dissertation and papers regarding CPG, Ezekiel documented and published many different numerical simulations [21]. Included in these publications are many details regarding the simulation set-up, reservoir geometry, and well control. This allows us to reconstruct equivalent models closely within our own open-DARTS environment, with the aim of comparing and verifying our models against Ezekiel's.

4.1. Aquifer verification

We start our analysis with the simplest case, the aquifer reservoir. Given that we approximate this reservoir as a two-component system, this is a natural starting point. Following "Numerical analysis and optimization of the performance of CO₂-Plume Geothermal (CPG) production wells and implications for electric power generation" [23], we reconstruct a similar reservoir of equivalent dimensions and properties.

The reservoir has a slight anticlinal structure and is modelled as a quarter of a quasi-five-spot pattern. The reconstructed version for this master thesis is shown in figure 4.1. More details regarding the reservoir are given in table 4.1. In Ezekiel's study the production well bottomhole pressure is set to be 180 bar for the base case. Additionally, the system is mass-rate limited, and thus, on exceeding the maximum production rate of 30 kg/s, the pressure will be adjusted accordingly. Initially, the production well is shut in, and CO_2 is only injected and not produced. When the CO_2 saturation around the production well reaches a threshold value we start production.

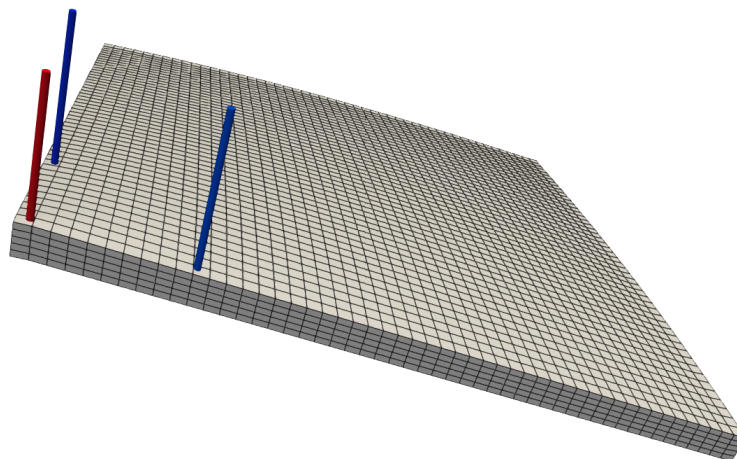


Figure 4.1: Quarter model of the reconstructed reservoir as presented in [23]. The anticlinal structure is exaggerated in this image for visualization purposes.

Parameter	Value
n_x	55
n_y	55
n_z	5
Height (H)	100 m
Length (L)	2250 m
Permeability x	100 mD
Permeability y	100 mD
Permeability z	50 mD
Porosity	0.20
Reservoir top depth	2500 m
Heat capacity	1000 J/(kg·K)

Table 4.1: Reservoir and simulation parameters

Running a simulation with our model using the prescribed setup, we can compare the models and see if they produce comparable results. We compare two parameters: the amount of electricity produced and the temperature at the production well. These results are shown in figure 4.2.

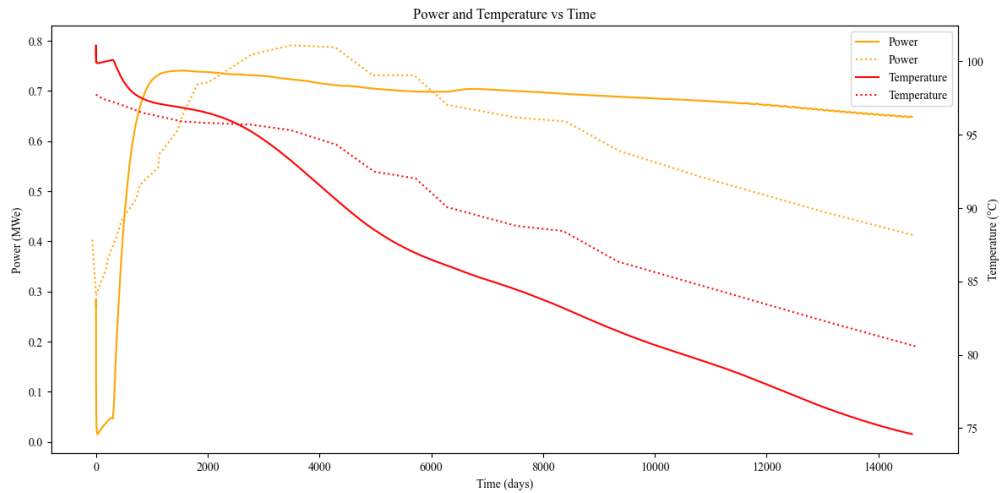


Figure 4.2: Bottom hole temperature and Electrical power produced. The dotted line is reference data from Ezekiel, the solid our results.

Discussion

As this reservoir has been reconstructed based on a textual description in a paper, deviations are expected. Our wellbore model is simplified compared to the wellbore model used in the validation study. One major source of deviation is the fact that we neglected the PE state, which was included in the reference study. Because our results diverged for this stage, we have decided to neglect this and start directly with the production. Our results slightly overestimate the peak energy production, which is to be expected as the simplified wellbore model neglects frictional losses. Our temperature drops more quickly than in the validation study; this can be explained by a lower net-to-gross ratio resulting from the omission of the PE stage. The validation study defines the inlet temperature exclusively for the wellhead and not at reservoir depth. Our reconstructed temperature may be incorrect, which significantly impacts the rate of heat extraction as well. Overall, the power model seems to match the validation model quite closely.

4.2. Gasfield validation

Ezekiel has published other work using the same reservoir but for CPG in gas reservoirs [22]. We can thus repeat this analysis but then for this environment. However, this study, with its many phases and injection schemes, is exponentially harder to reproduce. As open-DARTS has been part of multiple benchmark studies which have suggested its modelling to be quite accurate [28], we are mostly interested in validating our power model. When we do a simplified approach, we yield what Ezekiel refers to as a "Peak Gross Power" of 2.049 MWe. Ezekiel finds a value of roughly 2 MWe.

4.3. Regarding other simulators

Considering CPG's multi-physical nature, modelling it accurately and capturing all phenomena is not a trivial endeavour. CO_2 's highly complex multi-phase behaviour with its phase-dependent properties and state-sensitive phase partitioning requires a potent simulator to be modelled.

Two commonly used simulators for CPG are the THOUGH2 simulator developed by the Lawrence Berkeley National Laboratory, using the EOS7C library for the EOS [22] [24] or the ECO2N EOS [2] [31]. Another commonly used simulator is the CMG-GEM simulator [43] [17] [69], a privately developed simulator. Both simulators are very capable they have many strengths and some limitations. Comparison with each other and open DARTS is thus of value.

4.3.1. THOUGH2

THOUGH2 is a multiphase fluid and heat flow simulator for fluids within reservoirs [50]. Initially developed for geothermal reservoir engineering and nuclear waste disposal [51], it has been used for much more than just those applications and studies using it for practically the whole spectrum of reservoir engineering. TOUGH2 has a structure that allows the user to choose an EOS module that calculates the secondary variables specific to the to-be-modelled problem.

EOS7C

EOS7C is an EOS TOUGH2 module that uses a cubic equation of state. It allows for the modelling of a system with the following components: water, C1, and tracer, which is assumed to not affect gas properties, and a non-condensable gas. For CPG purposes this non-condensable gas is taken as CO_2 . Water is modelled as two components, pure water and brine [46]. This EOS, which includes C_1 as gas-component besides CO_2 is suited for CPG modelling in depleted gas reservoirs. Some limitations of this EOS are the following:

- Because water is modelled as two separate components, modelling salt precipitation is not possible. As often with CO_2 within water-containing reservoirs, salt precipitation could influence the performance of CPG [44].
- CO_2 is modelled as a non-condensable gas, phase change can thus not be modelled.
- Effects of brine salinity on gas solubility are neglected.
- The effects of dissolution of gas components within the brine on the density are neglected.

ECO2N

An alternative to EOS7C is ECO2N. ECO2N is a similar EOS Module developed for CO_2 sequestration within saline formations. It matches experimental data up to 600 bar and 110 ° C. It includes the possibility to model salt precipitation and dissolution. It does, however, note that data for properties of brine and CO_2 is scarce, and cross-validation is limited. [52]. Some limitations of this simulator are:

- The aforementioned maximum temperature is within the temperatures expected in reservoirs of interest for a CPG play. This limits its applicability. However, studies using this simulator outside this range have been conducted [2]. Hinting that its usability may be broader as presented here.
- Just like EOS7C it is not capable of phase transitions for CO_2 .
- As opposed to EOS7C it does not allow for the modelling of an already present gas such as C1. Limiting this EOS exclusively to be used for saline aquifer reservoirs and not the wider EGR/EOR possibilities.

4.3.2. CMG-GEM

CMG-GEM is a widely used privately developed reservoir simulation software. Its main use is for unconventional hydrocarbon recovery and CCS. It markets itself as a simulator capable of simulating a wide range of physics including more complex phenomena such as geomechanics and the modelling of foam. Despite these strengths, there are also some limitations:

- While GEM has a thermal option [14] it has some drawbacks. When comparing TOUGH2-ECO2N and GEM the temperature responses differ under the same reservoir [70]. Partly caused by the not modelled thermal effects of mutual dissolution of CO_2 and brine.

- GEM uses many empirical mixing rules, which need to be calibrated [42].
- GEM allows the users to choose between two EOS, PR and SRK [14]. More accurate EOS for our purposes exist.

4.3.3. Open-DARTS comparison

In table 4.2 we summarize our comparison of these simulators and Open-Darts.

	EOS7C	ECO2N	CMG-GEM	Open-DARTS
Multi-phase	✓	✓	✓	✓
Non-isothermal	✓	✓	✓	✓
Components sytem	CH ₄ -H ₂ O + trace	CO ₂ -H ₂ O-NaCl	flexible	flexible
Water vaporization	limited	✓	✓	✓
CO ₂ condensation	X	X	✓	~
Geomechanics	X	X	✓	✓
Open-source	X	X	X	✓

Table 4.2: Comparison of several simulators used for the numerical modeling of CPG. After [15].

5

Simulation strategy

The nature of our results depends highly on the reservoirs we study. What geometries do we study, and how do we populate these models? How do different injection-production schemes impact performance, and how do different environments affect the results? Referring back to our research questions, we can construct the following experiments.

5.1. PE phase

Before we start injection, there is practically no CO_2 present in the reservoir and thus a PE phase is required. CO_2 does have much higher mobility than water has, and therefore, only limited CO_2 saturation needs to be reached around the production well for it to become more mobile than the water. For the aquifer, we do take the saturation as the goal for the PE phase. For the gas phase, this situation is more nuanced as producing the already present gas is not undesirable. As the turbine inlet pressure is derived from the production well BHP, sufficient pressure build-up is required before a on surface pressure differential will develop between the wells. For the gas environments, the aim of the PE phase will thus be to pressurize the reservoir.

5.2. Wells

For the well control, we take a pressure-limited mass rate approach. With the wells producing at a certain target mass rate but clipped for a maximum and minimum pressure. In previous studies rate control is generally chosen to be preferred over pressure control, as rate control allows for a more constant and realistic energy output. A downside of using mass rate is that the effective volume in your reservoir can change quite significantly because of different phase densities in the production well, introducing unwanted pressure perturbations. The benefit of mass rate over volumetric is that it is independent of the state, while volume is. The injection well is perforated at the bottom half and the producer is perforated at the top half for the aquifer type. Because this drives density-driven convection. For the gas field type, the wells are perforated at the same depth.

5.3. Simulation parameters

We utilize a static time-stepping regime based on experimental experience, yielding the best results. This regime implies a gradually increasing timestep, which causes good stability and little wasted Newton iterations. The time step per iteration for the base case can be seen in figure 5.1. Our time stepping is rather conservative as too aggressive time stepping in our experiments caused the model to model collapse, a failed simulation. The drops in the figure are related to very near proximity to an outputting time of the grid files.

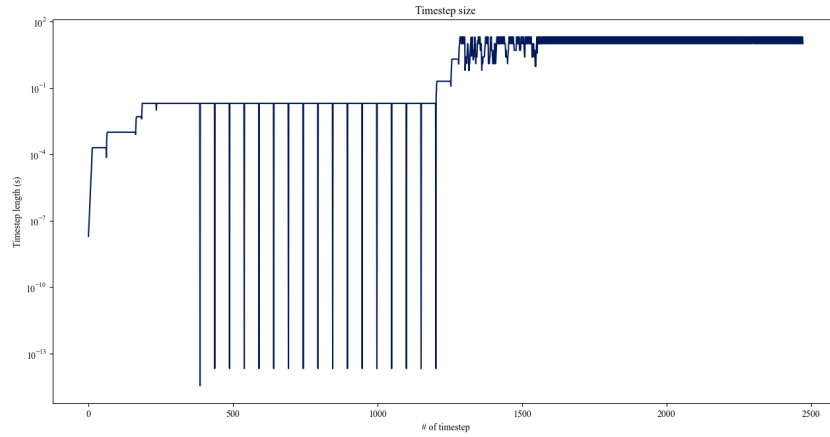


Figure 5.1: Timestep sizes during the simulation.

5.4. Experimentation plan

For our experiments, we construct a simple reservoir with properties similar to that commonly found in literature. The reservoir model parameters are given in table 5.1.

Parameter	Value
Number of cells in x-direction (n_x)	50
Number of cells in z-direction (n_z)	50
Number of cells in y-direction (n_y)	10
Reservoir height (H)	100 m
Reservoir length (L)	1000 m
Permeability in x-direction k_x	100 mD
Permeability in y-direction k_y	100 mD
Permeability in z-direction k_z	50 mD
Porosity (ϕ)	0.20
Reservoir top depth	2500 m
Base injection mass rate	30 kg/s
$S_{w,c}$	0.2
$S_{g,r}$	0.1
Geotherm	37 °C/km
Pressure	Hydrostatic

Table 5.1: Reservoir model parameters.

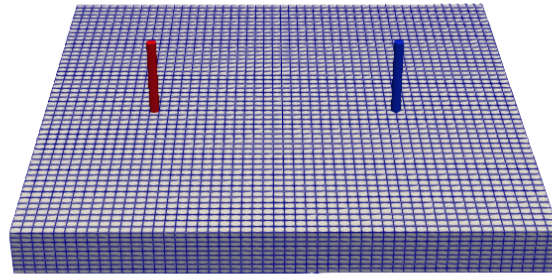


Figure 5.2: The reservoir mesh, with the well locations indicated. Blue is the injection well, and red is the production well.

5.4.1. Reservoir type comparison

For the first experiment, we compare both types of reservoirs, aquifers and gas fields. For the aquifer type we instantly start production and injection with equal mass rates of 30 kg/s. For the gas field, a PE stage of 10 years is included. This is necessary as due to the much lower density and higher compressibility of C_1 , electricity generating would not be possible when production would immediately start. These experiments will also function as a base case for both types.

5.4.2. Injection-production scheme

For this subquestion, we will conduct two types of experiments. We will experiment with the influence of the PE stage on performance and investigate how, and if, a seasonal demand impacts the performance of the reservoir.

PE stage

We will study how the PE stage influences the behaviour and performance of the reservoir. This means we vary the amount CO_2 injected before production starts. For the aquifer type, we vary the length of the PE stage into four stages. We do experiments with PE stages of; 0, 5, 10, and 15 years. During this time, 30 kg/s of CO_2 is continuously injected into the aquifer. Once this stage ends, 30 kg/s will also be the target for production. For the gas field type, we opted for a different approach. We vary the amount of CO_2 injected during a fixed period of 10 years. We experiment with 30 kg/s, 45 kg/s and 60 kg/s mass rates.

Seasonal electricity production

For our second experiment, we utilize our coupled model to control our production well by the electrical energy generated. We will introduce a sinusoidal demand for a year. We will compare these results with the scenario that the electricity demand was constant throughout the year. The aim is to find if, and how, seasonal demand affects the longevity of the reservoir.

5.4.3. Study of the environment

Great aquifer

In this environment, we add an aquifer to the bottom of the reservoir. We dub this scenario "Great Aquifer". What we are interested in is how a big connected aquifer that allows water to flow back into the reservoir or buffer pressure changes impacts the reservoir performance. To model this, we add an underburden of a single block that acts as a quasi-infinite reservoir. We will also include this reservoir for the PE experiment in the gas field, as the inclusion of such a reservoir increases the stability of the simulation. Why this is the case will be addressed in the discussion.

Stratified geology

Lastly, we want to experiment with a stratified reservoir. Stratified reservoirs are especially interesting for geothermal applications as while the low permeability layers do not conduct fluids; they do conduct heat to the more permeable layers. To capture a more accurate picture of this stratified behaviour, we increase the vertical resolution of our reservoir model from 10 to 20 cells for the experiment. Permeability for a single cell is kept isotropic. This model is an upscaled version of the model used in “Open-source Simulation Study for Direct Use Geothermal Systems” [12].

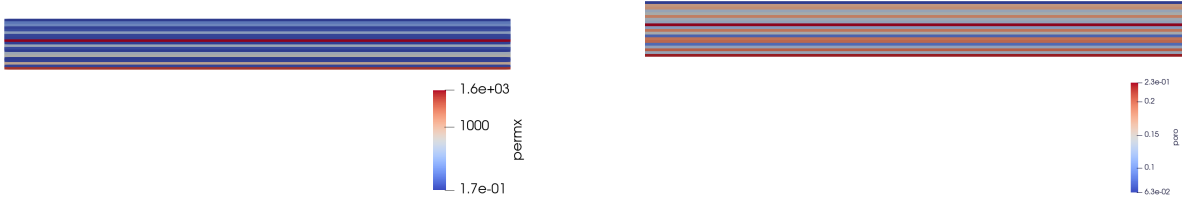


Figure 5.3: Permeability in miliDarcy and porosity for the stratified reservoir.

6

Results

In this chapter, we display the results of our experiments. We start with an exposition of our results for base case of each type, then proceed with derived scenarios beginning with the "Great Aquifer" experiment. We then continue to the results from the experiments with the PE stages, and then the seasonal electricity production results are discussed. Lastly, we show the results for the stratified environment.

6.1. Base case

It is beneficial to analyze the base case to understand how and why the reservoir and produced fluids develop during CPG operation. Here, we show results for the simplest experiment within this study.

6.1.1. Aquifer

For this base case, we haven't included a PE stage and instantly start production. As a result, our produced fluids consist almost exclusively of water initially, and thus, the CO_2 replacement ratio will be relatively low. This can be seen in figure 6.5. This also causes the flow regime not to be annular, as can be explained by the higher water cut, but for the significant part of the simulation, annular flow is achieved, as can be seen in figure 6.3. Looking at the electricity production, we see a sudden and strong increase which quickly levels out; this can be explained by the abrupt and strong breakthrough of CO_2 to the production well.

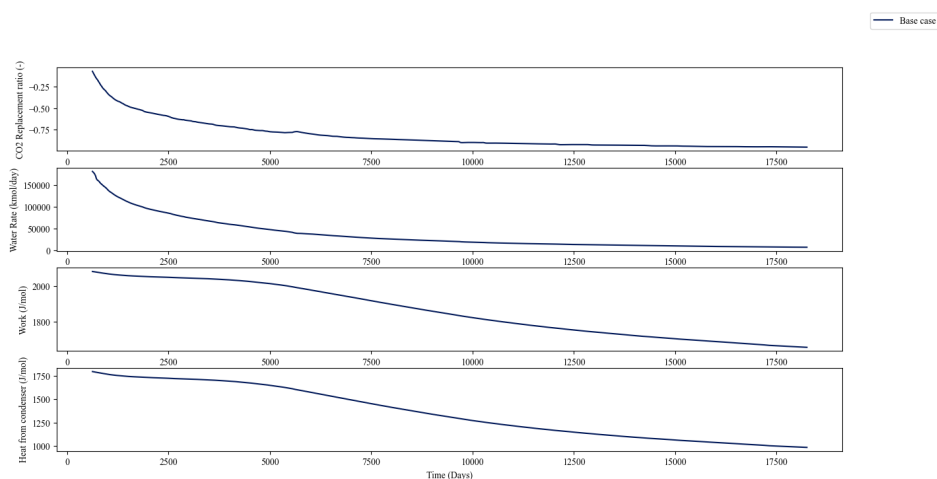


Figure 6.1: Key parameters for the aquifer base case.

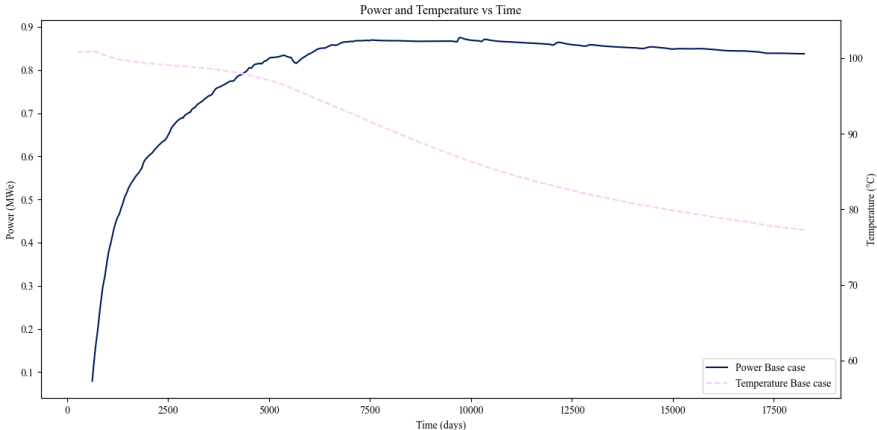


Figure 6.2: Electricity production and temperature at the production well for the aquifer base case.

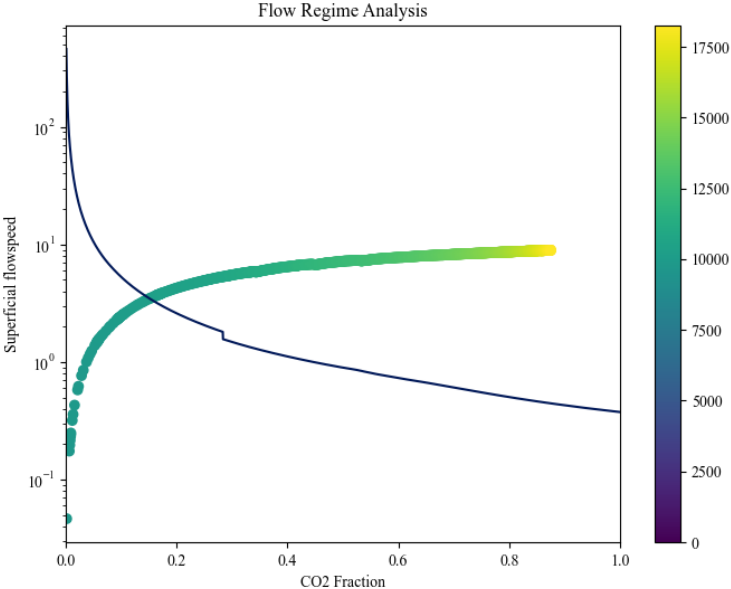


Figure 6.3: Flow regime in the production well. The line corresponds to the boundary of the annular flow regime. The color represents to days of the simulation.

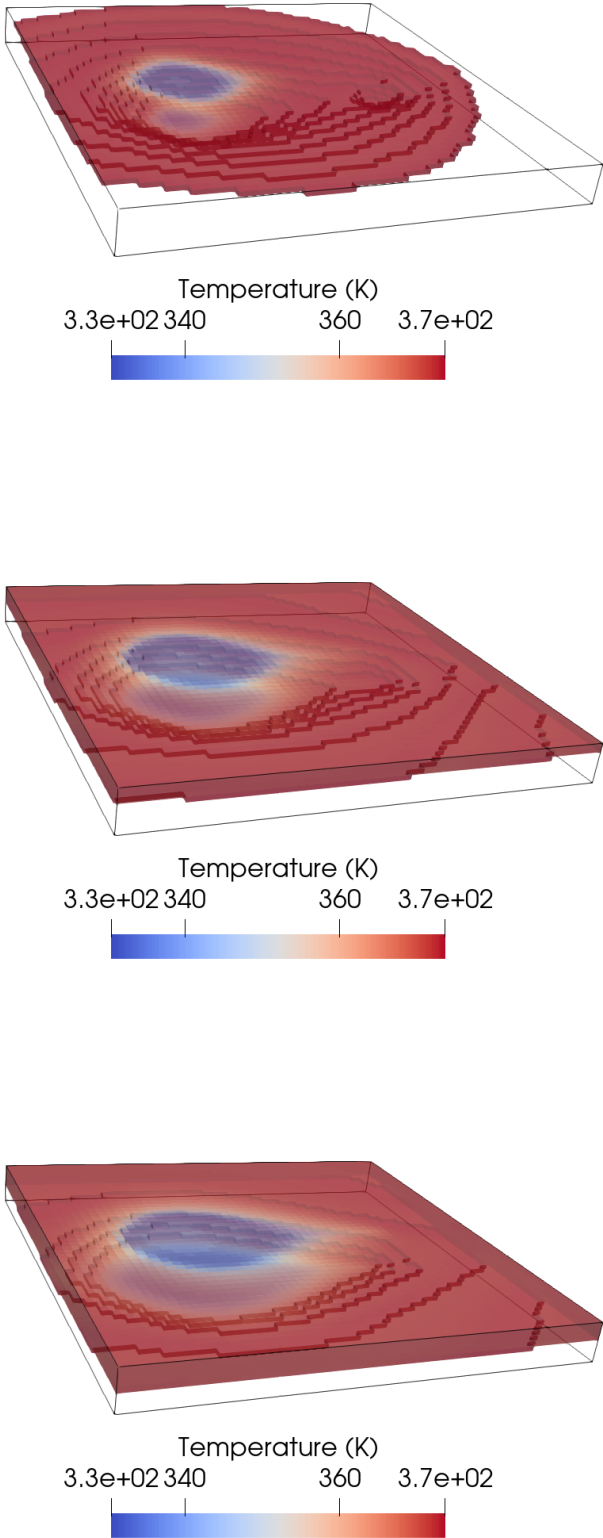


Figure 6.4: Migrating temperature plume. Cells that have a CO_2 molar fraction of more than 8% are shown for 500, 1000, and 1500 days.

6.1.2. Gasfield

Because the C_1 gas has a lower density than the CO_2 and is very compressible, we first included a 10-year PE stage to ensure proper reservoir pressurisation. For this base model, the initial water saturation is 5%. This is below the connate saturation. Upon opening the wells, there is a spike of fluids produced, including CO_2 . After this initial spike, the CO_2 molar fraction gradually increases, causing the total energy produced to increase gradually. What is interesting to note is that despite no mobile water being present, around a thousand kilomole of water is produced per day. All this water must thus be caused due to dry-out effects.

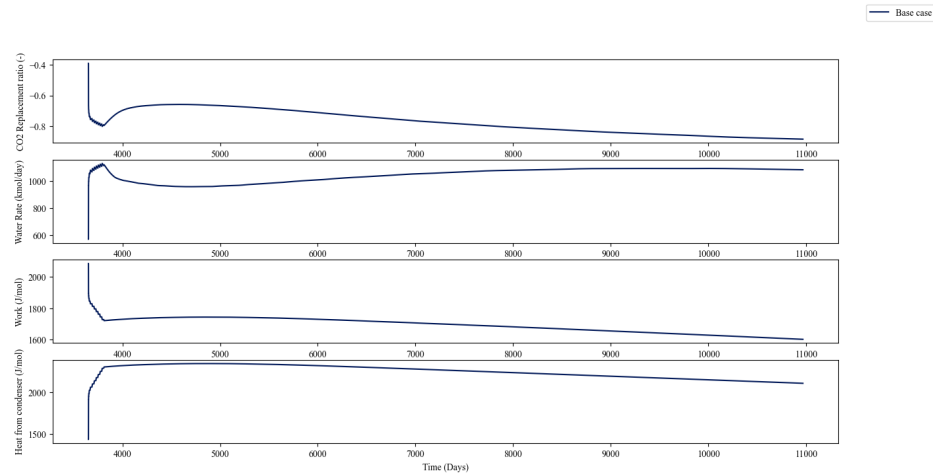


Figure 6.5: Key parameters for the gas field base case.

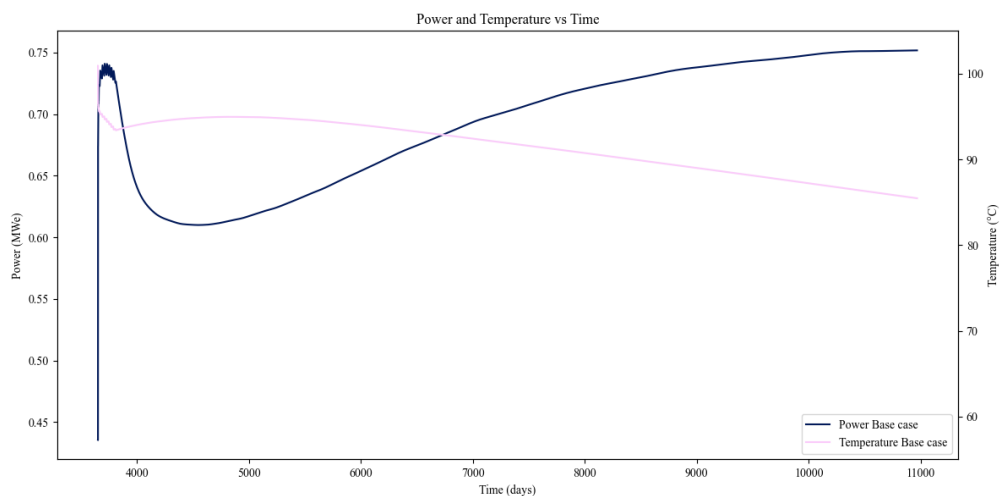


Figure 6.6: Electricity production and temperature at the production well for the gas field base case.

If we look at the plume development in figure 6.7 we see a very different development than for the aquifer plume. Instead of floating to the top as the CO_2 does, it sinks to the bottom of the reservoir as the already present components are less dense than the injected CO_2 . We see that the plume does not spread behind the production well. We can thus assume that any C_1 still present there is practically unrecoverable in this reservoir.

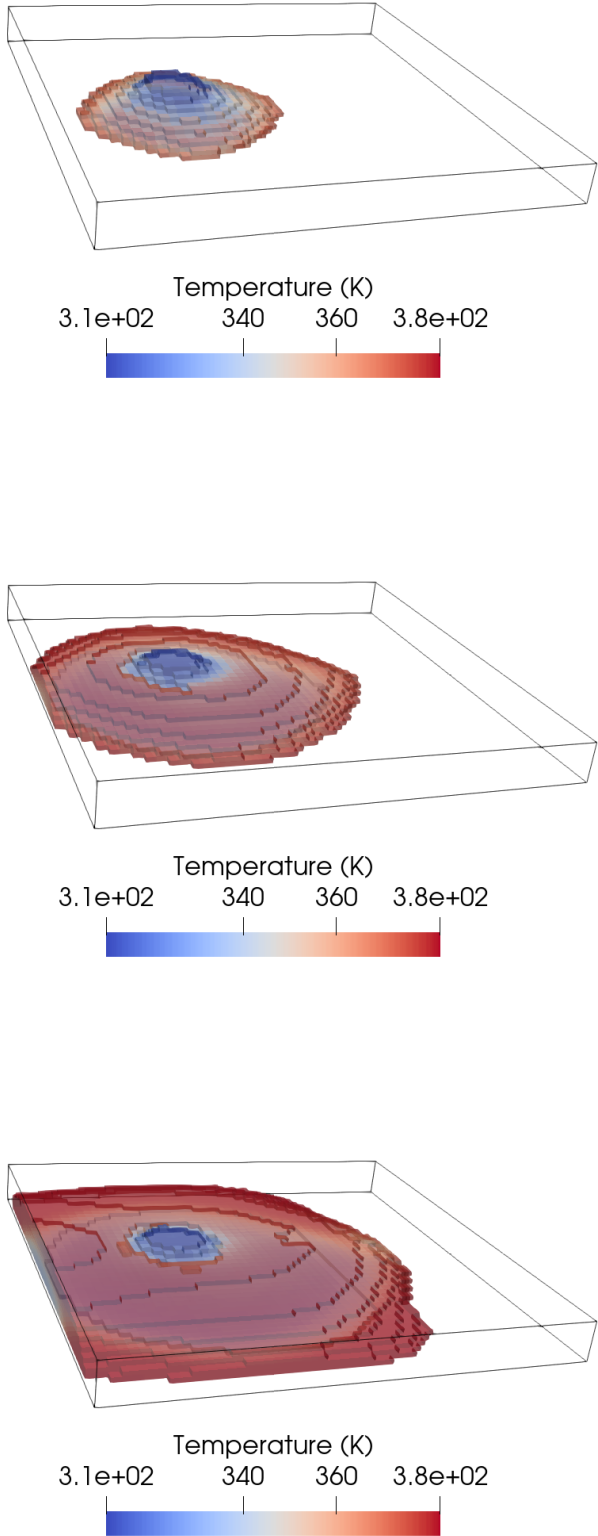


Figure 6.7: Migrating temperature plume, cells that have a higher than 25% molar fraction CO₂ are shown for 1000, 2000 and 4000 days.

6.2. Great Aquifer

Our first environment is the addition of a great connected aquifer to the model. This will introduce much more water to both environments and introduce a pressure buffer, which can absorb some of the pressure buildup in the reservoir.

6.2.1. Aquifer

As expected, the introduction of a "Great aquifer" causes more water to be produced as shown in figure 6.8. The higher pressure and inflowing water also cause the production well to stay at higher pressure and temperature and thus produce more energy per mole of produced CO_2 . Interestingly enough, this does not lead to a higher energy production caused by the higher water cut in the production well.

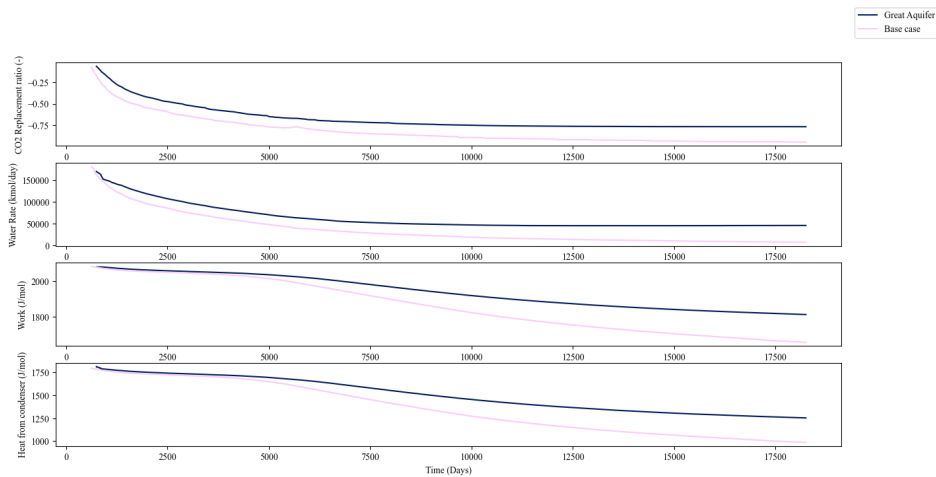


Figure 6.8: Key parameters for this scenario.

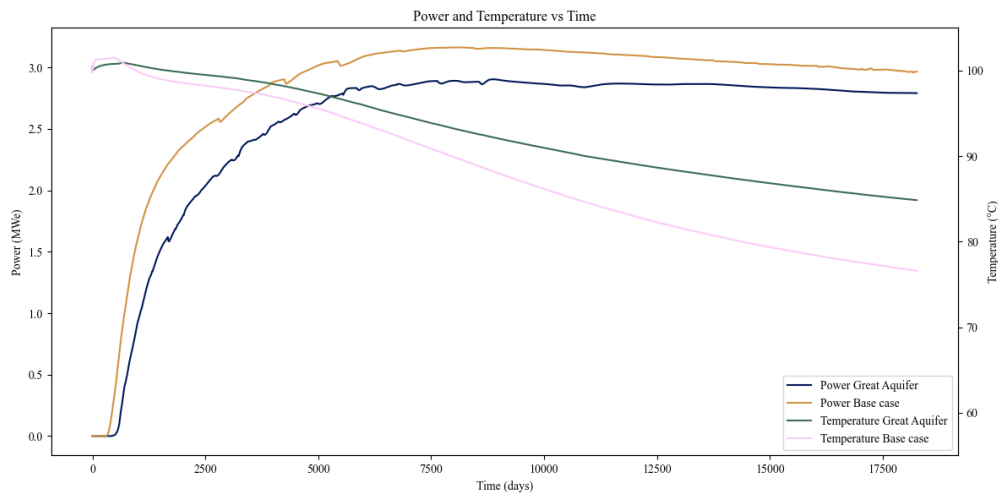


Figure 6.9: Electricity production and temperature at the production well.

6.2.2. Gas field

Here, we observe a much starker difference than for the aquifer type. As can be seen in figure 6.10. The main difference lies in the consistently lower amount of produced CO_2 , as can be seen in the replacement ratio. The pressure buffering of the aquifer prevents the reservoir from building up pressure. This results in a much lower electricity generation. Due to the lower amounts of produced fluids, we also have less cooling. As can be seen in figure 6.11.

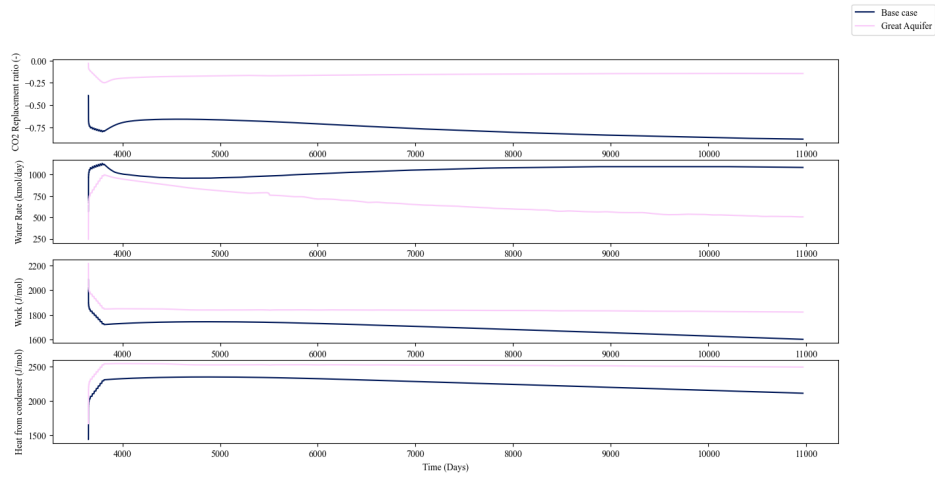


Figure 6.10: Key parameters for the gas field with a connecting aquifer.

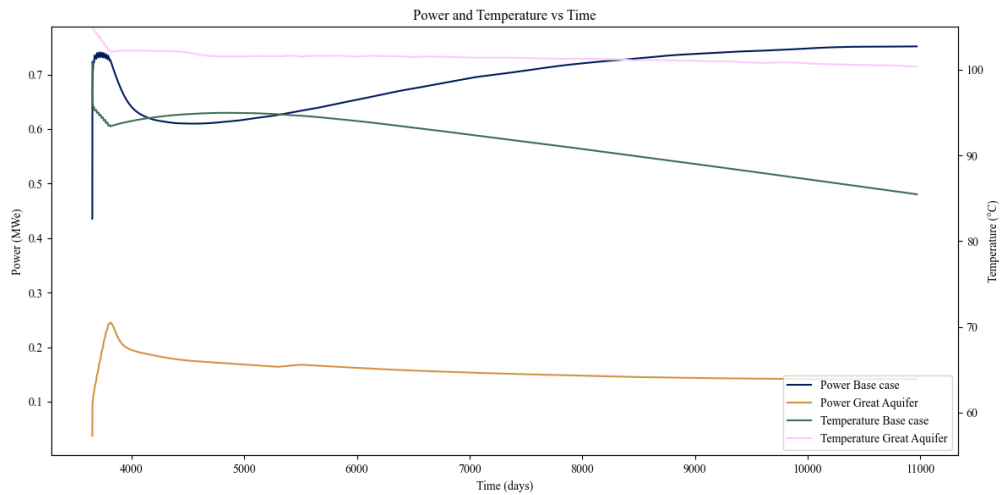


Figure 6.11: Electricity production and temperature at the production well for the gas field with connecting aquifer.

6.3. Plume establishment

In this section, we show the results of our experiments with alternating the PE period. We will take the base case as a reference and compare the results. We start by looking at the aquifer type and then later continue with the gasfield type.

6.3.1. Aquifer

Plume development

We start by analysing the behaviour of the plume in the reservoir for different PE times. Figure ?? shows the cooling caused by the injection of CO₂. We clearly see that as long as the production well is off the CO₂ spreads in all directions evenly. Once the production well opens the CO₂ it starts to channel in that direction. We also see that due to the longer PE time, a larger volume of the reservoir is swept and heat is extracted. In this experiment the bottom half of the well has been perforated, this leads to a stronger cooling around the bottom of the reservoir than at the top at the injection well. Due to buoyancy effects, the plume migrates upwards, causing the cooling to be mostly at the top of the reservoir once it reaches the production well.

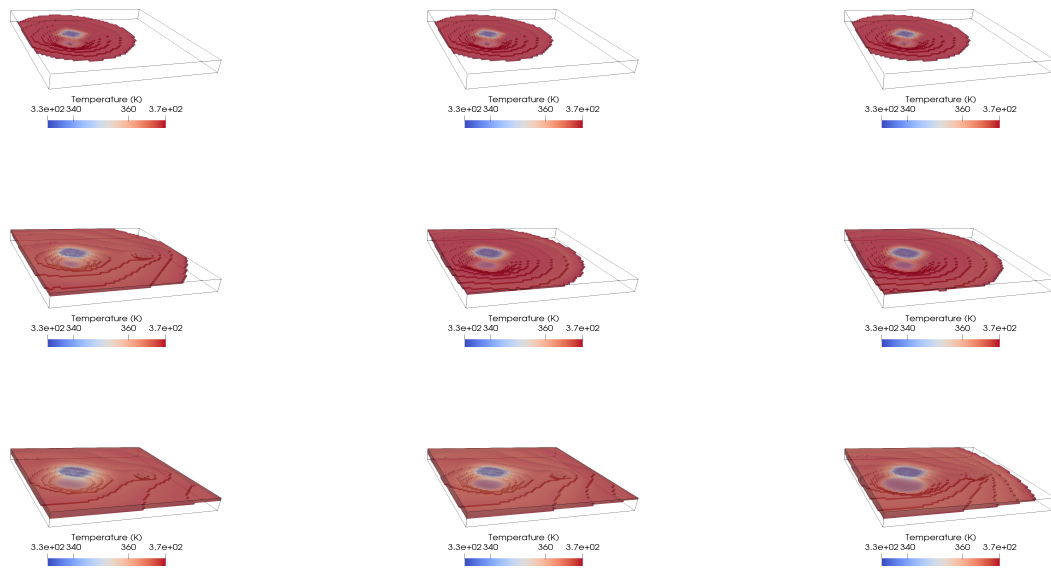


Figure 6.12: Migrating temperature plume, cells that have a higher than 8% molar fraction CO_2 are shown for 5000, 10000 and 15000. Left to right correspond to PE stages of 5, 10, and 15 years. The zero years is identical to the "Great Aquifer" case.

Energy production

Here we explore how the PE phase impacts the performance of the reservoir. During the PE phase, the pressure in the reservoir steadily increases and the plume migrates closer to the production well. In figure 6.13 the electricity and temperature curves are plotted for all scenarios. Because the absolute time for when electricity production begins is of course dependent on the prior PE time, we have set the moment of first electricity production as time is 0 for each scenario.

Comparing the different power profiles against each other, we see that the scenarios differ at the beginning of production to then converge at later times. We see that the initial energy production strongly correlates with the plume establishment time. This can be explained by two factors: there is higher pressure in the reservoir and thus higher pressure at the turbine inlet and due to the high pressure, the bottom hole pressure is clipped as described in the well control section, which will result in a greater (CO_2) mass rate.

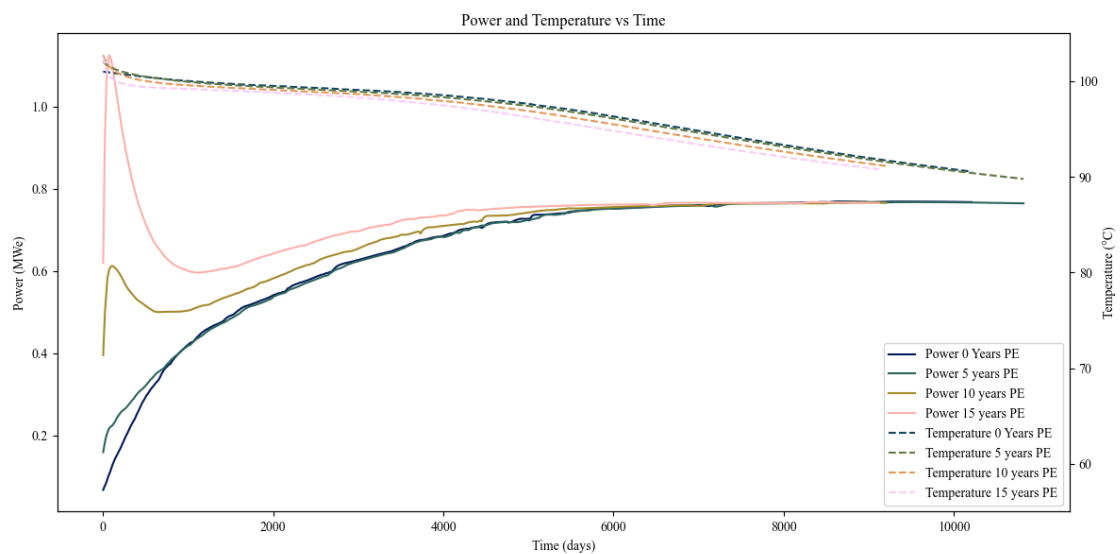


Figure 6.13: Electricity production and temperature at the production well for the aquifer field for several PE stages.

6.3.2. Gas field

For this type, the plume development is very similar to that of the base case and will not be addressed. For this scenario, we see a trend that is very similar to that of the aquifer type. With more electricity produced with a longer PE, resulting in a consistently higher electricity produced. This is shown in figure 6.15. In figure 6.14 you can clearly observe that the energy boost is driven by higher amounts of CO_2 produced and less water.

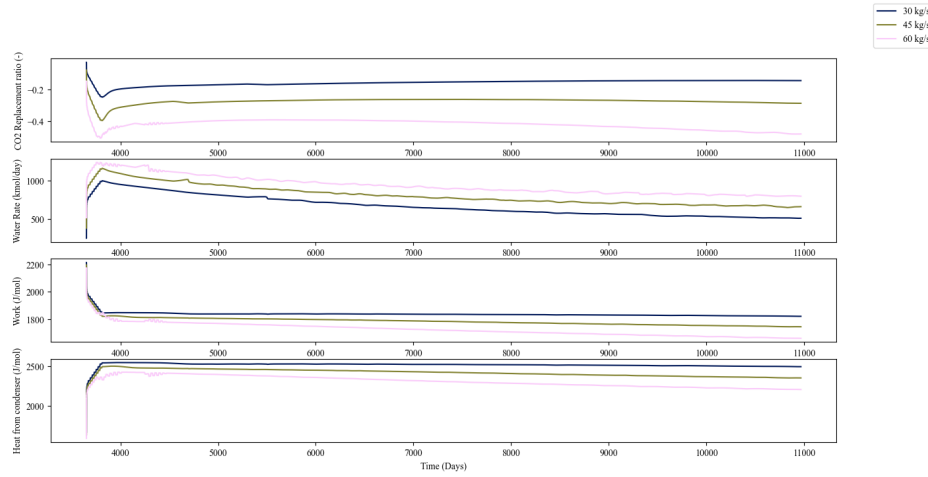


Figure 6.14: Key parameters for the gas field with different PE stages.

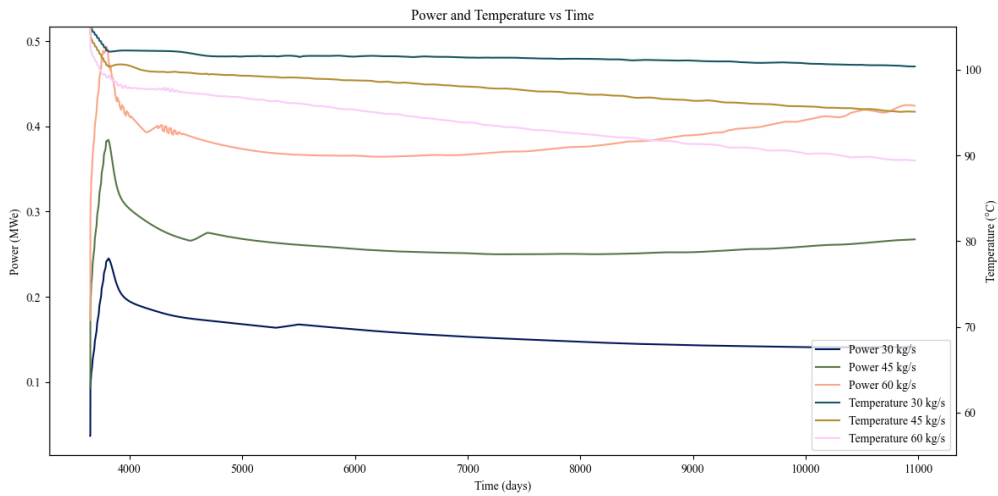


Figure 6.15: Electricity production and temperature at the production well for the gas field for several PE stages.

6.4. Seasonal electricity

In this experiment, we based our production scheme on electricity production. More specifically, we modelled a season-based electricity consumption. Here, we took a sinusoidal electricity demand over a period of a year with an average demand of 0.6 MWe and an amplitude of 0.3 MWe. These results can be seen in figure 6.16. We see the temperature fluctuate inversely with the electricity production, this is an artefact caused by the fluctuating pressure at the bottom of the borehole which influences the temperature of the entering gas.

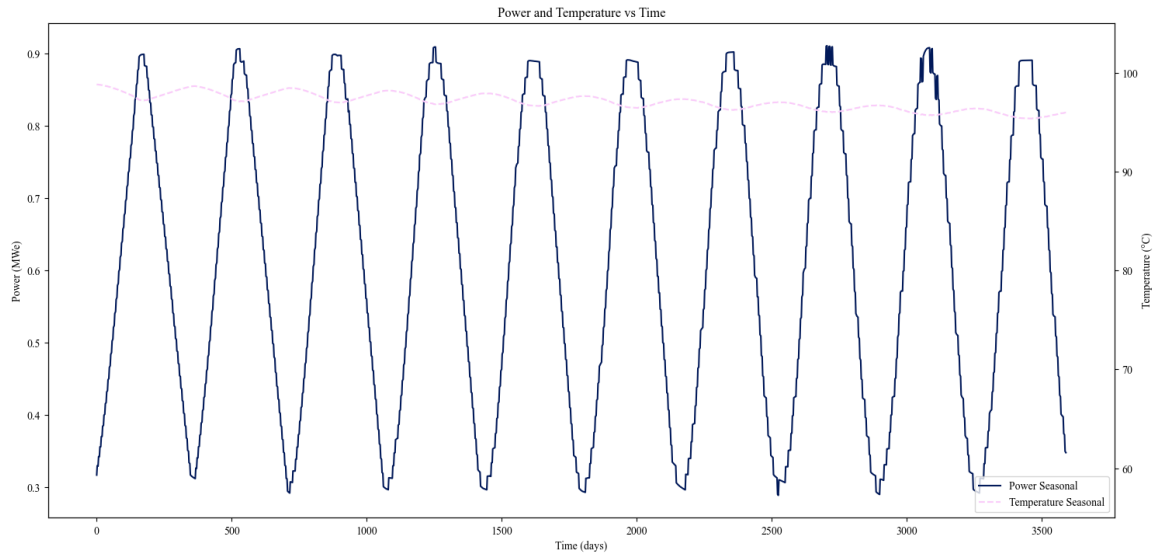


Figure 6.16: Electricity production and temperature at the production well the seasonal demand scenario.

We compare the injection scheme of figure 6.16 with a constant electricity production of 0.6 MWe, the average electricity production in the previous graph to determine whether a production scheme like this actually influences longevity, we compare the bottom-hole temperature of the production well. This will correspond to an equal amount of energy produced over the whole period. If we compare the temperature drop for these both schemes, we see a less than 0.5K higher drop for the seasonal scheme.

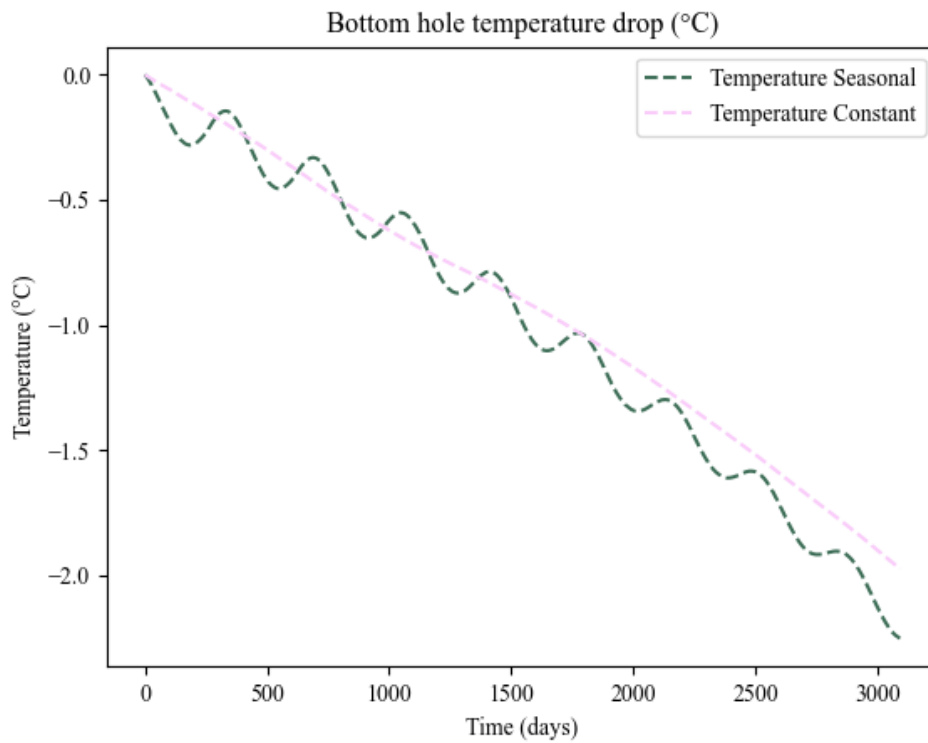


Figure 6.17: Borehole temperature drop for constant and seasonal energy production.

6.5. Stratified geology

In this experiment, we investigated a heavily stratified reservoir. The development of the plume and temperature can be seen in Figure 6.18. As can be observed, the plume is now much more spread out within each permeable stratified layer, with the impermeable layers preventing the CO_2 from floating towards the top of the reservoir.

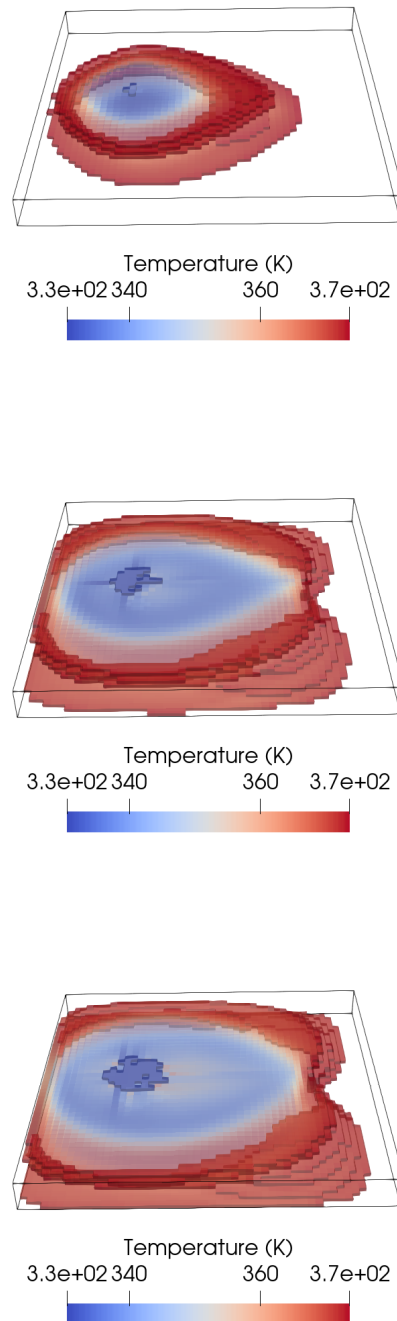


Figure 6.18: Migrating temperature cells that have a higher than 8% molar fraction CO_2 are shown for 3000, 6000 and 9000 days.

When we compare the several parameters for this reservoir with the base case, we see quite notable differences, as can be seen in figure 6.19. Energy production starts earlier than for the base case; this is caused by the channelling of the CO₂ in the permeable layers towards the production well. Initial energy production per mole is equal to the base case, but it quickly drops off. Eventually, due to the CO₂ cut increasing yet the temperature remaining constant due to conductive effects, the energy production keeps increasing.

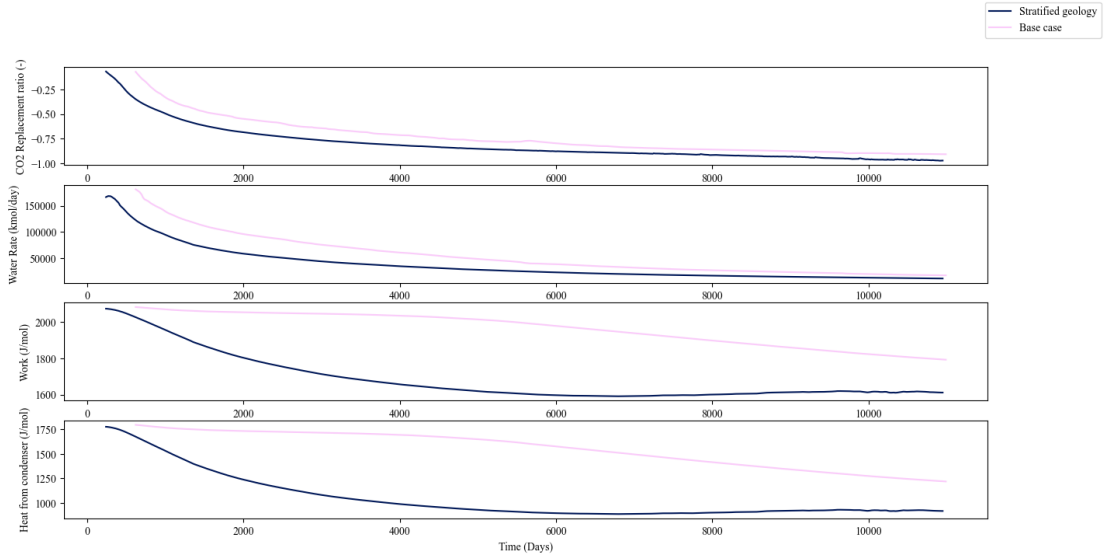


Figure 6.19: Key parameters for the stratified reservoir environment.

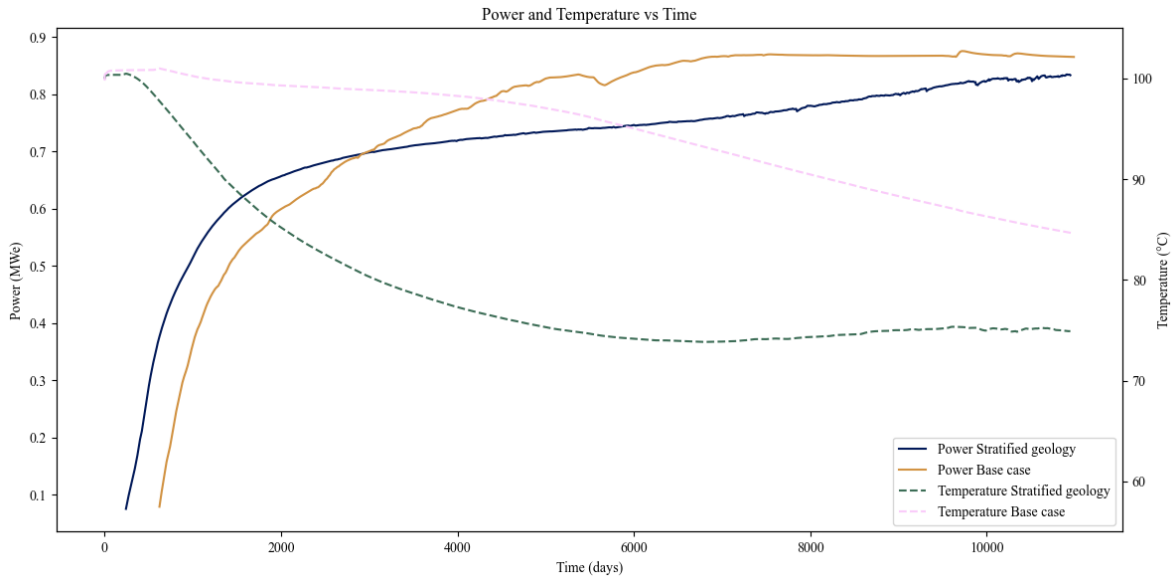


Figure 6.20: Electricity production and temperature at the production well for the stratified reservoir environment.

7

Discussion

Oil field

In the current study, we have focused on two types of reservoirs: aquifers and gas fields. Initially and until a late stage of the study, we had opted to include a third oil field type of reservoir in this study. However, we experienced instabilities in the enthalpy calculations using the EoS for hydrocarbon mixtures. Causing our models to give us unrealistic temperature values. While the model did function properly under isothermal conditions, including flash calculations. The decision was made to drop this type of reservoir from our analysis as an isothermal study of geothermal would be of little value. In our oilfield hydrocarbon mixtures, we had included n-decane. The PR EoS is known to fail to accurately estimate the enthalpy of mixtures with heavy oils, such as n-decane [34]. A first step for future research regarding CP in (depleted) oilfields could be to implement a better relationship or adjusted EoS to better match the properties of heavy oils.

Cycle model

The reservoir model was the focus of this study. However, we have included a simplified model for the wells and surface infrastructure. We have shown that this model matches similar studies quite closely. It is also much faster, thanks to the implementation of the DARTS-Flash library and OBL techniques. In the end we only included exsolution effects for the turbine, and neglected it for the wells. We have decided to do this because our provisional approach our values deviated from literature. An approach that seemed promising but fell flat due to instability in the volume calculations is using the isentropic expansion coefficient as defined in “Calculation of Joule-Thomson and isentropic expansion coefficients for two-phase mixtures” [5]. Instead of working our way backwards to the isentropic solution as we do now, using this coefficient, we can work our way forward. For every “expansion step”, one should be able to recalculate the phase fraction distribution and, given a small enough step size, converge to the real solution.

Wells

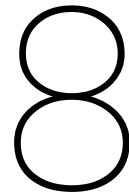
For this study the decision was made to circumvent the default wells option that open-DARTS offers and use an alternative and simpler approach instead. This decision was made because the standard implementation suffered from instabilities for systems with more than two components which made injection and production practically impossible. For the injection in the gas field type of reservoirs we used a technique that did not use well-cells but instead added CO_2 to the designated reservoir cells manually. This technique only allowed us to do a volumetric or mass rate approach. Where would we want to model i.e. the self-sustained thermosiphon, an pressure controlled injection well might be a better approach.

For the production well we opted for a pressure bounded mass rate approach. As rate control in open-DARTS is set per phase, constant recalibration of the rate control based on the changing phase fraction was necessary. While this worked quite well during relatively constant production we encountered complications when phase fractions or mass-rates changed quickly. As this recalibration could only be done smoothly, too big changes would cause the model to collapse, this recalibration sometimes could

not be done fast enough. Resulting in strong, unrealistic peaks in the massrate. In practise these kind of peaks would be filtered out by friction losses in the borehole, but as our model did not include those effects there was no balancing force.

Reservoir Composition

In most of our experiments we have included a connecting aquifer. One reason for this has been that during experimentation, we found that if components third in order or higher were not omnipresent, instability in the saturation correction occurred. One way we used to circumvent this was setting the third component to be the most commonly present component throughout the simulation. For the gas field this was H_2O , which also gave us the most stable runs. However during continued production and injection problems occurred around the wells. With H_2O presence diminishing to very low values due to dry-out, problems arised. An additional fix has been to add a connecting aquifer to most of our gas field scenarios, guaranteeing H_2O presence throughout the simulation.



Conclusion and recommendations

This master's thesis investigated the performance of a CO_2 plume geothermal (CPG) in both aquifer and gas field reservoirs. It investigated the impact of different injection and production schemes and how different conditions impacted the performance.

Model

A model capable of efficiently modelling the full cycle of CO_2 plume geothermal operations was built. We have exhibited that the open-Darts framework can easily be extended to the well and surface infrastructure. Our reservoir model is capable of simulating the multiphase thermal behaviour for both two and three components. We have compared our model against the literature and found very similar results despite the simplistic wellbore and turbine model.

Different types of reservoirs

Comparing the types of reservoirs, aquifers and gas fields, there are stark contrasts in gains and benefits. Based on the performance metrics we determined, we see some clear differences. Aquifer scenarios produce significantly more water than gas fields as was probably expected. However, the biggest difference lies in energy production. While electrical energy production per mole is quite similar, producing significant amounts of CO_2 with a high bottom hole pressure proves to be difficult. The energy generated by the turbine depends for a significant part on the pressure of the produced fluids. For the Aquifer this is not a limitation, as the reservoir is pressurized from the start and injection of CO_2 only further increases the pressure. For gasfields, however, this is a big hurdle; during conventional gas production, the pressure in the reservoir will drop. While this drop has been very limited in previous studies, realistic values may lay below a hundred bar. Leaving you with a scenario where copious amounts of CO_2 may need to be injected before any electricity can be produced at all, What makes things worse is the fact that CO_2 is significantly denser than C_1 and thus to replace the original gas in place to reach the same pressure one needs to inject much of CO_2 per tonne of C_1 produced. In this report, we have not considered the question of whether depressurization of a gas reservoir back to its original pressure is desirable regarding caprock integrity and seismic risks. However, these seem to be additional cons to the CPG potential for gas fields. We can conclude that while aquifers produce more water and provide no extra hydrocarbons, a CPG play in aquifers appears to be much more viable than in depleted gasfields.

Injection regimes

Our second research question was how different injection and production schemes impact the performance of the reservoir. We see for both types of reservoirs that greater amounts of CO_2 injected prior to CO_2 production yield better results. More electrical energy is generated and less water is produced. While we see that for gas fields, this higher efficiency sustains, we see that for the aquifer type, the energy generated converges. A seasonal production scheme does not seem to severely impact the longevity of the reservoir. With only a little bit more temperature drop than the steady electricity generation. An important note should be made here that in the seasonal electricity production scheme, much

higher flow rates are reached in the production well. As in our model, we neglected frictional; this does not cause problems. In reality, though, this will negatively impact such an injection-production scheme.

Environments

For environments, we looked at two environments that we expected to impact reservoir performance. A connecting aquifer and a stratified reservoir. The connecting aquifer negatively impacted the reservoir by hindering pressure build-up and introducing more water into the production well. The stratified reservoir didn't give us a univocal picture. While less electricity is generated per mole CO_2 , the net electricity generated is comparable to the homogenous case. The highly permeable layers allowed the CO_2 to more easily reach the production well less water needed to be displaced. This once again shows that geological heterogeneities are very influential.

Recommendations

For future research and as this technology matures and moves closer to a field demonstration, there are a few things worth investigating and improving on. Firstly the reservoirs we have considered here have been very homogenous and isotropic. Like for all forms of reservoir exploitation geological heterogeneities play a big role in the performance, possibly even bigger than the difference in types as studied here. The permeability and porosity fields of siliciclastic and carbonate reservoirs differ immensely. Additionally, the distribution of facies for different depositional environments, i.e. deltaic and fluvial reservoirs, deviate substantially. These kinds of effects should all be considered and compared once the candidates get narrowed down.

Secondly, in this study, we have looked exclusively at the performance based on physical parameters such as electricity produced and waste water extracted. To compare this technology quantitatively with other sources of renewable energy and techno-economic analysis should be made including a levelized cost of electricity (LCOE) comparison. Determining this LCEO will be no trivial task. As not only the revenues from the electricity and heat generation must be considered. But also an inclusion of the costs/revenue of the CO_2 storage and the economic benefits of the possible additional hydrocarbon recovery.

Lastly, it is important to continue work on open-DARTS before the CPG study continues. For this study, we have used exclusively the Python interface open-DARTS offers and have not touched the C++ core. We made this decision because of the ease and flexibility Python offers and to ensure compatibility with the ever-evolving core. However, stability in determining the composition correction of systems with more than two components should be improved. Another topic that should be investigated is how to allow for more drastic well control changes. Especially during CO_2 breakthrough we often ran into stability problems.

References

- [1] Benjamin Adams et al. "An Analysis of the Demonstration of a CO₂-based Thermosiphon at the SECARB Cranfield Site". In: *46th Annual Stanford Geothermal Workshop (SGW 2021)*. 2021.
- [2] Benjamin M Adams et al. "A comparison of electric power output of CO₂ Plume Geothermal (CPG) and brine geothermal systems for varying reservoir conditions". In: *Applied Energy* 140 (2015), pp. 365–377.
- [3] Benjamin M Adams et al. "On the importance of the thermosiphon effect in CPG (CO₂ plume geothermal) power systems". In: *Energy* 69 (2014), pp. 409–418.
- [4] Nikolay N Akinfiev and Larry W Diamond. "Thermodynamic model of aqueous CO₂-H₂O-NaCl solutions from- 22 to 100 C and from 0.1 to 100 MPa". In: *Fluid Phase Equilibria* 295.1 (2010), pp. 104–124.
- [5] Ababakari Oumarou Ali, Daniel Broseta, and Dan Vladimir Nichita. "Calculation of Joule-Thomson and isentropic expansion coefficients for two-phase mixtures". In: *Science and Technology for Energy Transition* 78 (2023), p. 20.
- [6] Ian H Bell et al. "Coolprop: An open-source reference-quality thermophysical property library". In: *ASME ORC 2nd International Seminar on ORC Power Systems*. 2013.
- [7] Charles de Beus. "Reservoir Considerations for Carbon-Dioxide Plume Geothermal in Depleted Gas Reservoirs". In: (2021).
- [8] F Böhmer et al. "NextGen Geothermal Power (NGP)-A new sCO₂ based geothermal concept". In: *Proceedings of the European Geothermal Congress*. 2022.
- [9] Neima Brauner. "Churn flow". In: *Multiphase Science and Technology* 8.1-4 (1994).
- [10] Donald W Brown. "A hot dry rock geothermal energy concept utilizing supercritical CO₂ instead of water". In: *Proceedings of the twenty-fifth workshop on geothermal reservoir engineering, Stanford University*. 2000, pp. 233–238.
- [11] Michael Anthony Celia et al. "Status of CO₂ storage in deep saline aquifers with emphasis on modeling approaches and practical simulations". In: *Water Resources Research* 51.9 (2015), pp. 6846–6892.
- [12] Yuan Chen, Denis Voskov, and Alexandros Daniilidis. "Open-source Simulation Study for Direct Use Geothermal Systems". In: *PROCEEDINGS, 49th Workshop on Geothermal Reservoir Engineering Stanford University* (2024).
- [13] Chevron Australia Pty Ltd. *Gorgon Project Carbon Dioxide Injection System Pipeline and Wells Operations Environment Management Plan: Summary*. Environmental Management Plan Summary. Perth, Western Australia: Chevron Australia, 2023.
- [14] CMG. *GEM user manual*. 2019.
- [15] Michiel Creusen. "Near wellbore effects induced by CO₂ injection and the influence on injectivity in depleted gas reservoirs". In: *TU Delft repository* (2018).
- [16] Guodong Cui et al. "Geothermal energy exploitation from depleted high-temperature gas reservoirs by recycling CO₂: The superiority and existing problems". In: *Geoscience Frontiers* 12.6 (2021), p. 101078.
- [17] Guodong Cui et al. "Whole process analysis of geothermal exploitation and power generation from a depleted high-temperature gas reservoir by recycling CO₂". In: *Energy* 217 (2021), p. 119340.
- [18] Francois De Kerret et al. "Two-phase flow pattern recognition in a varying section based on void fraction and pressure measurements". In: *IOP Conference Series: Earth and Environmental Science* 49 (Nov. 2016), p. 052015. DOI: 10.1088/1755-1315/49/5/052015.

- [19] Marius Dewar et al. "Impact potential of hypersaline brines released into the marine environment for CCS reservoir pressure management". In: *International Journal of Greenhouse Gas Control* 114 (2022), p. 103559.
- [20] Ola Eiken et al. "Lessons learned from 14 years of CCS operations: Sleipner, In Salah and Snøhvit". In: *Energy procedia* 4 (2011), pp. 5541–5548.
- [21] Justin Ezekiel. "Assessment and optimization of geological carbon storage and energy production from deep natural gas reservoirs". PhD thesis. ETH Zurich, 2020.
- [22] Justin Ezekiel et al. "Combining natural gas recovery and CO₂-based geothermal energy extraction for electric power generation". In: *Applied Energy* 269 (2020), p. 115012.
- [23] Justin Ezekiel et al. "Numerical analysis and optimization of the performance of CO₂-Plume Geothermal (CPG) production wells and implications for electric power generation". In: *Geothermics* 98 (2022), p. 102270.
- [24] Justin Ezekiel et al. "Sensitivity of reservoir and operational parameters on the energy extraction performance of combined co₂-egr-cpg systems". In: *Energies* 14.19 (2021), p. 6122.
- [25] Mark R Fleming, Benjamin Adams, and Martin O Saar. "Using sequestered CO₂ as geothermal working fluid to generate electricity and store energy". In: *World Geothermal Congress (WGC 2020+ 1)*. ETH Zurich. 2020, p. 37024.
- [26] Mark R Fleming et al. "Flexible CO₂-plume geothermal (CPG-F): Using geologically stored CO₂ to provide dispatchable power and energy storage". In: *Energy Conversion and Management* 253 (2022), p. 115082.
- [27] Mark R Fleming et al. "Increased power generation due to exothermic water exsolution in CO₂ plume geothermal (CPG) power plants". In: *Geothermics* 88 (2020), p. 101865.
- [28] Bernd Flemisch et al. "The FluidFlower validation benchmark study for the storage of CO₂". In: *Transport in Porous Media* 151.5 (2024), pp. 865–912.
- [29] Sofianos Panagiotis Fotias, Spyridon Bellas, and Vassilis Gaganis. "Optimizing geothermal energy extraction in co₂ plume geothermal systems". In: *Materials Proceedings* 15.1 (2023), p. 52.
- [30] Barry M Freifeld et al. "Demonstration of Geothermal Energy Production Using Carbon Dioxide as a Working Fluid at the SECARB Cranfield Site, Cranfield, Mississippi". In: *Proceedings of the forty-first workshop on geothermal reservoir engineering, Stanford University, Stanford*. 2016.
- [31] Nagasree Garapati et al. "CO₂-plume geothermal (CPG) heat extraction in multi-layered geologic reservoirs". In: *Energy Procedia* 63 (2014), pp. 7631–7643.
- [32] Jil Hansper et al. "Assessment of performance and costs of CO₂ Plume Geothermal (CPG) Systems". In: *European Geothermal Congress*. 2019.
- [33] Mahmoud Hefny et al. "Synchrotron-based pore-network modeling of two-phase flow in Nubian Sandstone and implications for capillary trapping of carbon dioxide". In: *International Journal of Greenhouse Gas Control* 103 (2020), p. 103164.
- [34] Desheng Huang and Daoyong Yang. "Improved enthalpy prediction of hydrocarbon fractions with a modified alpha function for the Peng-Robinson equation of state". In: *Fuel* 255 (2019), p. 115840.
- [35] MD Jager, AL Ballard, and ED Sloan Jr. "The next generation of hydrate prediction: II. Dedicated aqueous phase fugacity model for hydrate prediction". In: *Fluid phase equilibria* 211.1 (2003), pp. 85–107.
- [36] Mark Khait and Denis Voskov. "Adaptive parameterization for solving of thermal/compositional nonlinear flow and transport with buoyancy". In: *SPE Journal* 23.02 (2018), pp. 522–534.
- [37] Sebastian Köhlert. *CPG Subsea Power Plant—When solutions come together*. Tech. rep. Copernicus Meetings, 2024.
- [38] Yongge Liu et al. "A method to recover natural gas hydrates with geothermal energy conveyed by CO₂". In: *Energy* 144 (2018), pp. 265–278.
- [39] M.L. Michelsen and J.M. Mollerup. *Thermodynamic Models: Fundamentals & Computational Aspects*. Tie-Line Publications, 2007. ISBN: 9788798996132.

- [40] Banafsheh Nematollahi et al. "Evaluation and optimization of a horizontal well-triplet for CO₂ plume geothermal harvest: Comparison between open and close reservoirs". In: *Journal of Hydrology* 623 (2023), p. 129811. ISSN: 0022-1694. DOI: <https://doi.org/10.1016/j.jhydrol.2023.129811>. URL: <https://www.sciencedirect.com/science/article/pii/S0022169423007539>.
- [41] Dan Vladimir Nichita and Claude F Leibovici. "A rapid and robust method for solving the Rachford–Rice equation using convex transformations". In: *Fluid Phase Equilibria* 353 (2013), pp. 38–49.
- [42] Jean-Philippe Nicot et al. *Impact of CO₂ Impurities on Storage Performance and Assurance Report*. 2013.
- [43] Amir Mohammad Norouzi, Jon Gluyas, and Masoud Babaei. "CO₂-plume geothermal in fluvial formations: A 2D numerical performance study using subsurface metrics and upscaling". In: *Geothermics* 99 (2022), p. 102287.
- [44] Amir Mohammad Norouzi et al. "CO₂-plume geothermal processes: A parametric study of salt precipitation influenced by capillary-driven backflow". In: *Chemical Engineering Journal* 425 (2021), p. 130031.
- [45] Amir Mohammad Norouzi et al. "CO₂-plume geothermal: Power net generation from 3D fluvial aquifers". In: *Applied Energy* 332 (2023), p. 120546.
- [46] CM Oldenburg et al. "TOUGH2 Module for Carbon Dioxide or Nitrogen in Natural Gas (Methane) Reservoirs". In: *EOS7C version 1* (2004).
- [47] open-darts. *darts-flash*. <https://gitlab.com/open-darts/darts-flash>. 2023.
- [48] F.M. Orr. *Theory of Gas Injection Processes*. Tie-Line Publications, 2007. ISBN: 9788798996125.
- [49] Karsten Pruess. *ECO2N: A TOUGH2 fluid property module for mixtures of water, NaCl, and CO₂*. Vol. 497. Lawrence Berkeley National Laboratory Berkeley, CA, 2005.
- [50] Karsten Pruess. "TOUGH2-A general-purpose numerical simulator for multiphase fluid and heat flow". In: (1991).
- [51] Karsten Pruess, Curtis M Oldenburg, and GJ Moridis. "TOUGH2 user's guide version 2". In: (1999).
- [52] Karsten Pruess and Nicolas Spycher. "ECO2N—A fluid property module for the TOUGH2 code for studies of CO₂ storage in saline aquifers". In: *Energy conversion and management* 48.6 (2007), pp. 1761–1767.
- [53] Jimmy B Randolph and Martin O Saar. "Combining geothermal energy capture with geologic carbon dioxide sequestration". In: *Geophysical Research Letters* 38.10 (2011).
- [54] Jimmy B Randolph and Martin O Saar. "Coupling carbon dioxide sequestration with geothermal energy capture in naturally permeable, porous geologic formations: Implications for CO₂ sequestration". In: *Energy Procedia* 4 (2011), pp. 2206–2213.
- [55] Jimmy B Randolph et al. "Wellbore heat transfer in CO₂-based geothermal systems". In: *Geothermal Resources Council Transactions* 36 (2012), pp. 549–554.
- [56] J. Rogelj et al. "Mitigation Pathways Compatible with 1.5°C in the Context of Sustainable Development". In: *Global Warming of 1.5°C. An IPCC Special Report on the impacts of global warming of 1.5°C above pre-industrial levels and related global greenhouse gas emission pathways, in the context of strengthening the global response to the threat of climate change, sustainable development, and efforts to eradicate poverty*. Ed. by V. Masson-Delmotte et al. Cambridge, UK and New York, NY, USA: Cambridge University Press, 2018, pp. 93–174. DOI: 10.1017/9781009157940.004.
- [57] Martin O Saar et al. "How CCS can benefit from CO₂-Plume Geothermal (CPG)". In: *1st Caprock Integrity & Gas Storage Symposium 2024*. 2024, p. 13.
- [58] Amir Salehi, Denis V Voskov, and Hamdi A Tchelepi. "K-values-based upscaling of compositional simulation". In: *SPE Journal* 24.02 (2019), pp. 579–595.

- [59] Everett L Shock, Harold C Helgeson, and Dimitri A Sverjensky. "Calculation of the thermodynamic and transport properties of aqueous species at high pressures and temperatures: Standard partial molal properties of inorganic neutral species". In: *Geochimica et Cosmochimica Acta* 53.9 (1989), pp. 2157–2183.
- [60] A Rangriz Shokri et al. "Modeling CO₂ Circulation Test for Sustainable Geothermal Power Generation at the Aquistore CO₂ Storage Site, Saskatchewan, Canada". In: *2nd Geoscience & Engineering in Energy Transition Conference*. Vol. 2021. 1. European Association of Geoscientists & Engineers. 2021, pp. 1–5.
- [61] Xiaohui Sun et al. "Geothermal energy production utilizing a U-shaped well in combination with supercritical CO₂ circulation". In: *Applied Thermal Engineering* 151 (2019), pp. 523–535.
- [62] Yehuda Taitel, Dvora Barnea, and AE Dukler. "Modelling flow pattern transitions for steady upward gas-liquid flow in vertical tubes". In: *AIChE Journal* 26.3 (1980), pp. 345–354.
- [63] Denis Voskov et al. "open Delft Advanced Research Terra Simulator (open-DARTS)". In: *Journal of Open Source Software* 9.99 (2024), p. 6737.
- [64] Denis V Voskov. "Operator-based linearization approach for modeling of multiphase multi-component flow in porous media". In: *Journal of Computational Physics* 337 (2017), pp. 275–288.
- [65] Yang Wang et al. "An efficient numerical simulator for geothermal simulation: A benchmark study". In: *Applied Energy* 264 (2020), p. 114693.
- [66] Michiel Wapperom et al. "A Unified Thermal-Reactive Compositional Simulation Framework for Modeling CO₂ Sequestration at Various Scales". In: *SPE Reservoir Simulation Conference? SPE*. 2023, D021S010R005.
- [67] Richard H Worden. "Carbon Dioxide Capture and Storage (CCS) in Saline Aquifers versus Depleted Gas Fields". In: *Geosciences* 14.6 (2024), p. 146.
- [68] Tianfu Xu et al. "On fluid and thermal dynamics in a heterogeneous CO₂ plume geothermal reservoir". In: *Geofluids* 2017.1 (2017), p. 9692517.
- [69] Bora Yalcin, Justin Ezekiel, and P Martin Mai. "Potential for CO₂ plume geothermal and CO₂ storage in an onshore Red Sea Rift basin, Al-Wajj, Saudi Arabia: 3D reservoir modeling and simulations". In: *Geothermics* 119 (2024), p. 102966.
- [70] Mehdi Zeidouni, Jean-Philippe Nicot, and Susan D Hovorka. "Monitoring above-zone temperature variations associated with CO₂ and brine leakage from a storage aquifer". In: *Environmental earth sciences* 72 (2014), pp. 1733–1747.
- [71] Liang Zhang et al. "CO₂ injection for geothermal development associated with EGR and geological storage in depleted high-temperature gas reservoirs". In: *Energy* 123 (2017), pp. 139–148.
- [72] Zaman Ziabakhsh-Ganji and Henk Kooi. "An Equation of State for thermodynamic equilibrium of gas mixtures and brines to allow simulation of the effects of impurities in subsurface CO₂ storage". In: *International Journal of Greenhouse Gas Control* 11 (2012), S21–S34.